Digital design and additive manufacturing of structural materials in electrochemical and thermal energy storage systems: a review

Qing Liu, Ruihuan Ge, Chuan Li, Qi Li & Yixiang Gan

Published online: 01 Nov 2023.

Submit your article to this journal ☑

View related articles ☑

View Crossmark data ☑

Taylor & Francis
Taylor & Francis Group

REVIEW ARTICLE

OPEN ACCESS | Check for updates

Digital design and additive manufacturing of structural materials in electrochemical and thermal energy storage systems: a review

Qing Liu[a], Ruihuan Ge[b], Chuan Li[c], Qi Li[d] and Yixiang Gan[e,f]

[a]School of Mechanical Engineering, University of Science and Technology Beijing, Beijing, People's Republic of China; [b]Department of Chemical and Biological Engineering, University of Sheffield, Sheffield, UK; [c]School of Chemistry and Chemical Engineering, Shandong University of Technology, Zibo, People's Republic of China; [d]MOE Key Laboratory of Enhanced Heat Transfer and Energy Conservation, Beijing Key Laboratory of Heat Transfer and Energy Conversion, Beijing University of Technology, Beijing, People's Republic of China; [e]School of Civil Engineering, The University of Sydney, Sydney, NSW, Australia; [f]The University of Sydney Nano Institute (Sydney Nano), The University of Sydney, Sydney, NSW, Australia

ABSTRACT
Additive manufacturing is increasingly utilised in the energy conversion and storage field. It offers great flexibility to fabricate structural materials with improved physical properties, and other advantages such as material waste reduction, fabrication time minimisation, and cost-effectiveness. In this review, current developments in additive manufacturing of energy storage devices are discussed. The digital design approaches of structural materials and mainstream additive manufacturing techniques, including vat photopolymerization, powder bed fusion, material jetting, binder jetting, material extrusion, and directed energy deposition, are summarised. Then, a comprehensive review of recent advances in the electrochemical and thermal energy storage field is provided. In the end, an integrated framework considering digital design and additive manufacturing is proposed for a wide range of energy applications.

Abbreviations: ABS: Acrylonitrile Butadiene Styrene; AM: Additive manufacturing; AJ: Aerosol jet; CFD: Computational fluid dynamics; CLIP: Continuous liquid interface production; CNF: Carbon nanofiber; CNN: Convolutional neural network; DED: Directed energy deposition; DEM: Discrete element method; DOD: Drop-on-demand; DfAM: Design for additive manufacturing; DIW: Direct ink writing; DL: Deep learning; DLP: Digital light process; DMLS: Direct metal laser sintering; EBM: Electron beam melting; EBAM: Electron beam additive manufacturing; EHD: Electro hydrodynamic; FDM: Fused deposition modelling; FEA: Finite element analysis; FFF: Fused filament fabrication; GO: Graphite oxide; HDPE: High-density polyethylene; HTF: Heat transfer fluid; LB: Lattice Boltzmann; LDW: Laser deposition welding; LENS: Laser engineered net shaping; LHTES: Latent heat thermal energy storage; LFP: LiFePO$_4$; LTO: Li-Titanate; MFC: Microbial fuel cell; MnO$_2$: Manganese dioxide; ML: Machine learning; MJF: Multi jet fusion; MJP: Multi jet printing; MSCs: Micro-supercapacitors; MWNT: Multi-walled carbon nanotube; NCA: Nickel–Cobalt-Aluminium Oxide; PA: Polyamide; PBF: Powder bed fusion; PC: Polycarbonate; PCFC: Protonic ceramic fuel cell; PCMs: Phase change materials; PEGDA: Polyethylene glycol diacrylate; PEMFC: Polymer electrolyte fuel cell; PLA: Polylactic acid; PVDF: Polyvinylidene fluoride; SLA: Stereolithography; SLM: Selective Laser Melting; SLS: Selective laser sintering; SOFC: Solid oxide fuel cell; SPJ: Single Pass Jetting; SVM: Support vector machines; TES: Thermal energy storage; TPMS: Triply periodic minimal surface; TPU: Thermoplastic polyurethan; 3D: Three-dimensional; UV: Ultraviolet.

1. Introduction

The carbon dioxide emissions worldwide indicate that significant efforts need to be made to decarbonise the energy sector. More than 70 countries have made emission reduction plans to keep global warming less than 1.5 °C [1,2]. Developing efficient energy storage and conversion mechanisms are of critical importance to overcome the mismatch between renewable energy supply and energy demand. In the UK it is reported that 43 TWh energy storage capacity (~£165.3 billion investment) is needed to decarbonise the electricity supply [3].

The mainstream energy storage techniques can be classified into several types: electrochemical, thermal,

flywheel, compressed air, chemical, and hydrogen energy storage [4]. Compared with mechanical energy storage techniques, electrochemical and thermal energy storage techniques offer more flexibility and usually higher energy densities [4]. Structural materials are frequently employed in electrochemical and thermal energy storage systems for system efficiency improvement, safety, and durability. In energy storage systems, a micro-structural material usually consists of two or more phases. The spatial distributions of functional materials and pores are specifically designed and fabricated, to achieve superior performance compared with the properties of independent materials. Micro-structural materials are inherent features of typical energy storage systems. Examples include electrode structures in lithium-ion batteries [5], and phase change composite materials in latent heat thermal energy storage systems [6]. In the electrochemical and thermal energy storage systems, the system performance is heavily dependent on the multi-physics transport mechanisms. The function of structural material in these high-value energy systems involves essentially electrical, heat, and mass transport. Controlling the performance of such systems is subject to complicated multi-physics interactions across a large range of length scales. Rationale design of 3D structures can be used to attain improved properties. Previously, conventional manufacturing techniques such as slurry casting, extrusion, and rolling press were commonly used [5,7]. Take the Li-ion battery electrode as an example, electrode structures are fabricated by casting a mixture of active material particles and conductive additives onto a metallic current collector. The conventional manufacturing approach can hardly control the microstructure and material property distributions. Thus, the development and manufacturing of these materials has occurred through trial-and-error experimental investigation.

By fabricating components layer by layer, the additive manufacturing (AM) technique offers a way to fabricate complicated three-dimensional (3D) features with multiple materials at multiple scales [8,9]. Additive manufactured structures exhibit unique physical properties such as ultra-high stiffness [10], damage-tolerant properties [11], and improved thermal dissipation [12]. In recent years AM technologies have been used for energy generation, storage, and conversion [13,14]. For instance, selective laser melting (SLM) technology was used to manufacture advanced heat transfer devices such as heat exchangers and heat sinks [14]; direct ink writing (DIW) was commonly used to fabricate electrochemical energy storage devices with layered geometries [15]. The energy storage device performance is highly relevant to the intrinsic properties of energy materials,

microstructure design, and fabrication approach. For a typical energy storage device, the device performance is strongly affected by the coupled heat transfer, fluid flow, and electrochemical interactions. In this field, the device design and evaluation are usually based on empirical knowledge. In the last few years, new design strategies such as topology optimisation have been proposed [16]. Some review articles discussed relevant applications of additive manufacturing in thermal energy devices [17], and electrochemical systems [18]. However, few review articles addressed the digital design approach in this field. An integrated framework of digital design and additive manufacturing is helpful for the next generation energy storage techniques. Especially, application of digital design and additive manufacturing to maximise the electrochemical and thermal energy storage device performance needs to be addressed.

This review paper focuses on the contributions of novel digital design approaches and additive manufacturing in the energy storage field. The digital design and optimisation strategies of structural materials are firstly reviewed. Then, the mainstream AM techniques used for energy storage systems, i.e. vat photopolymerization, powder bed fusion, material extrusion, material jetting, binder jetting, and directed energy deposition, are summarised. AM can be used to fabricate various forms of structural materials, enabling the energy storage device design with optimised transport properties. Specifically, the electrochemical and thermal energy storage techniques are mainly reviewed. Eventually, future research directions are envisioned.

2. Digital design and optimisation strategies

To optimise the transport properties of energy devices, various structure design strategies, and optimisation algorithms could be adopted prior to additive manufacturing. Cellular structures such as human-made lattice structures, naturally occurring structures with varied sizes, porosity, and shapes are commonly used. The inverse design approach such as topology optimisation, data-driven can automatically generate devices with optimised performance prior to manufacturing. Typical applications of cellular structures and inverse design for energy storage systems are listed in the following Table 1.

2.1. Cellular structures

2.1.1. Synthetic lattice structures
Human-made cellular structures are usually generated via design algorithms. By Design for Additive Manufacturing (DfAM) algorithm, a 3D volume with desired internal lattice structures and volume fractions can be

Table 1. Digital design and optimisation strategies for energy storage systems.

	Design and optimisation strategies	Descriptions
Electrochemical energy storage	Cellular structure	Strut-based lattice [19,20]; TPMS structure [21–23]
	Inverse design	Topology optimisation [24]; Data-driven optimisation [25]
Thermal energy storage	Cellular structure	Strut-based lattice [26–28]; TPMS structure [29,30]
	Inverse design	Topology optimisation [12,16]; Data-driven optimisation [31]

built up. Figure 1 illustrates the most commonly used lattice structure unit cells created via the DfAM algorithm. These lattice structures are made up of solid struts, periodic or random interconnected networks. The lattice structure design is to find a balance between material consumption and physical properties. The resulting 3D volume design is usually affected by the size, type, orientation, spatial variations, and volume fraction of the periodic unit cells. Depending on the shape and internal structures, the lattice structures have distinct mechanical behaviours and transport properties. Previously, a major portion of research works in this field has been focused on the unique mechanical properties of these lattice structures. The unique transport properties of these lattice structures and applications in the energy storage field need to be further investigated. Results have shown that the bicontinuous triply periodic minimal surface (TPMS) surfaces can achieve the maximum transport of heat and electricity (Figure 1 (a-i)) [32]. TPMS structures have recently been used in typical energy storage devices, e.g. lithium-ion battery electrodes [21–23], and thermal energy storage devices [29]. Strut-based lattices (Figure 1 (k-q)) are commonly used for lightweight component design. It has been reported to be used in thermal energy storage systems for thermal conductivity enhancement [26–28]. Applications of these lattice structures in the energy storage field are reviewed in the following sections.

2.1.2. Naturally occurring structures
Apart from human-made lattice structures, cellular structures with complex topologies are very common in the natural environment. Those naturally occurring structures have been demonstrated to have some excellent properties. Bio-inspired structures could be designed to mimic the excellent properties of those naturally occurring structures [33]. Figure 2 illustrates some examples of naturally occurring structures that are commonly found in animal organs and growing plants. 3D

foam structures with random network/Voronoi network can be observed in human bones and bubbles (Figure 2 (a-b)). The honeycomb has a two-dimensional (2D) planar hexagonal structure (Figure 2 (c)). As demonstrated in Figure 2 (d-f), fractal structures could be observed in snowflakes and plants, which is useful for enhanced transport properties. To capture the complexity of these naturally occurring structures, design motifs at different length scales need to be explored. In addition, the rapid development of additive manufacturing technology provides a promising way to fabricate these complex structures in future [33].

2.2. Inverse design of structures

To generate structures with optimised properties, inverse design algorithms need to be considered. The inverse design approach offers the possibility to generate optimised designs outside the proposed design space in section 2.1. In the following, two main inverse design approaches in the energy device field are reviewed, i.e. functionality-driven topology optimisation approach and data-driven design.

2.2.1. Topology optimisation approach
Topology optimisation is a powerful tool for functionality-driven design. For obtaining a device with target properties, the design can freely evolve through the optimisation algorithm. In topology optimisation, optimal shapes are searched without a priori assumption. Usually, density approach or level-set approach is used to describe the material distributions with related physical properties during the optimisation [34]. A topology optimisation problem with partial differential equation (PDE) constraints can be mathematically described as:

$$\begin{aligned} \underset{\mathbf{s}}{\text{minimize}} \quad & t(\mathbf{s}, \mathbf{u}(\mathbf{s})) \\ \text{subject to} \quad & g_i(\mathbf{s}, \mathbf{u}(\mathbf{s})) = 0, \ i = 1, \ldots, N_{eq} \\ & h_j(\mathbf{s}, \mathbf{u}(\mathbf{s})) \leq 0, \ j = 1, \ldots, N_{ieq} \end{aligned} \quad (1)$$

where $\mathbf{u}$ is the degree of freedom vector, g_i is the generic equality constraint, and h_j is the generic inequality constraint.

A flow chart of the topology optimisation procedure is presented in Figure 3. The optimisation procedure starts from an initial shape with a homogeneous density distribution. Finite element analysis (FEA) is performed to address the physical issue. Afterwards, the gradient of the objective and constraints are calculated in the sensitivity analysis step. The design variables are updated via a gradient-based optimiser. Finally, the convergence will be checked until a convergence criterion is satisfied. The optimised layouts will be further post-
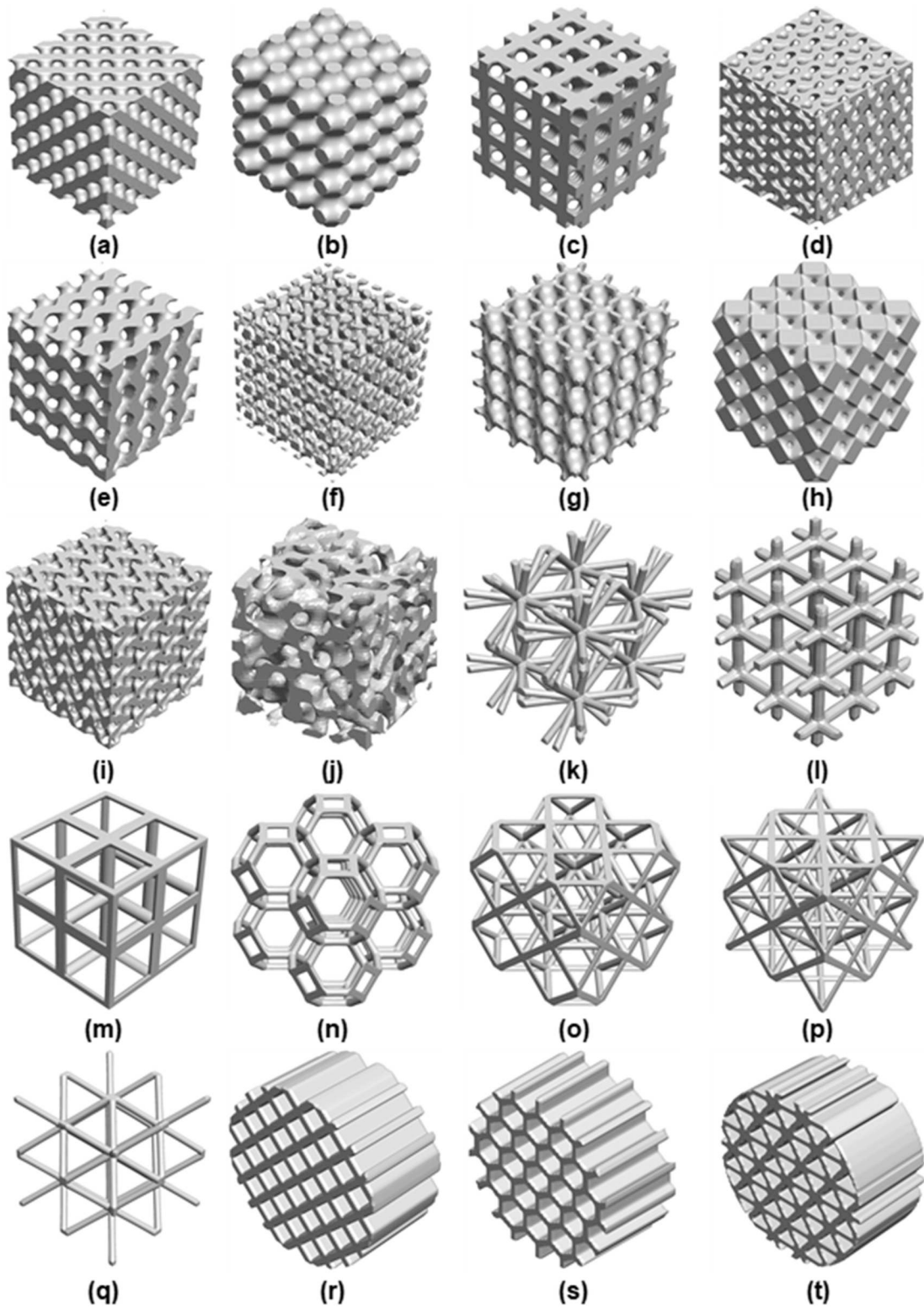
Figure 1. Various lattice structure types used for energy device: (a) TPMS Schwarz-D (b) TPMS Schwarz-P (c) TPMS Secondary I-WP (d) TPMS SplitP (e) TPMS Gyroid (f) TPMS Lidinoid (g) TPMS Neovius (h) TPMS Primary I-WP (i) TPMS FischerKoch (j) Stochastic structure (k) Hex truss (l) Face centre struts (m) Edge struts (n) Kelvin cell (o) Octagon struts (p) Face diagonal struts (q) Corner diagonal struts (r) Diamond (s) Hexagon (t) Triangle.

processed for manufacturing. Previously topology optimisation is mainly used for lightweight design and is recently gaining attention in the energy storage field [35]. Moreover, researchers have recently attempted to combine the topology optimisation approach with lattice structures to achieve superior performance [36].
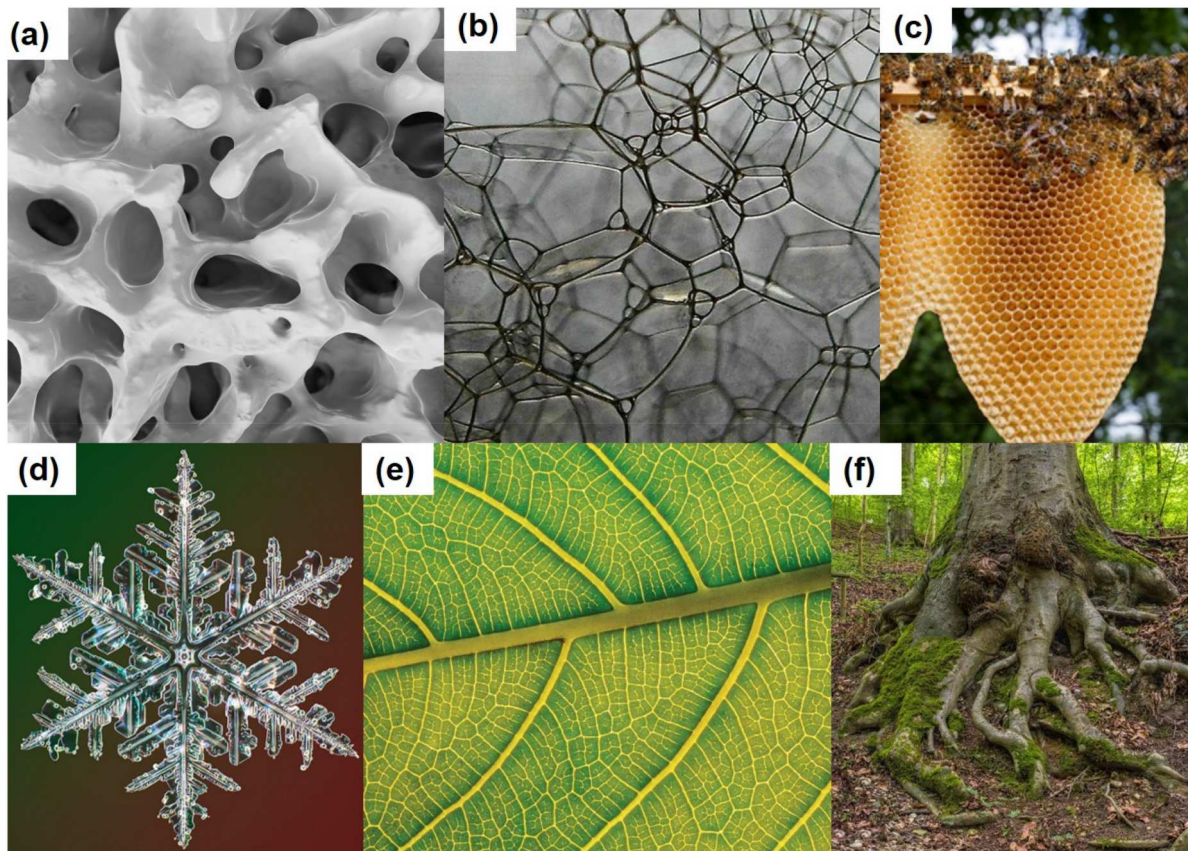
Figure 2. Examples of naturally occurring structures: (a) Human bone [41] (b) Bubbles [42] (c) Honeycomb [43] (d) Snowflake [44] (e) Leaf vein [45] (f) Plant root [46].

2.2.2. Data-driven design approach

Recently, data-driven design approaches have gained attention as an inverse design approach, e.g. machine learning algorithm, and deep learning driven generative design. It provides a promising way to identify the embedded process-structure–property correlations. With the rapid development of AI techniques, the data-driven design approach has been used in a variety of areas especially the molecular structure design of materials, e.g. nanoparticle packing design [37], and crystalline alloys [38]. Machine learning (ML) encompasses a series of supervised algorithms, such as kernel ridge regression, and support vector machines (SVM). The machine learning algorithm has been applied to the composition design of energy storage materials [7]. However, less work can be found in designing the micro-structures of energy storage devices. For the data-driven design approach, one major challenge is to fully capture the microstructure features. The deep learning (DL) approach can be considered as a subset of ML. One main advantage is that DL models like the convolutional neural network (CNN) can directly extract the structural features from the 3D images. Figure 4 illustrates a general process and flow chart of the DL-driven design

of structures with desired properties. The first step is the generation of a dataset with various topology, geo-metry, and relative density. The properties (electronic, structural, and thermal) of structures with varied compositions can be computed or experimentally measured firstly. Afterwards, the map between the material space and functionality space could be established via a data-driven design algorithm. For the DL approach, high-level features from prior layers could be extracted via a number of successive layers. This framework is used to design and discover new architectures with desired properties rationally and quickly. For the 'forward prediction', one can predict the material properties given the input physical structures. For the 'inverse design' of materials, appropriate structures can be determined with desired input physical properties. The DL data-driven models have been used to predict the mechanical properties of 3D microstructures [39,40]. However, typical applications in the energy storage field are still scarce.

2.3. Summary

Digital design and optimisation strategies have been used for energy storage systems. There have been
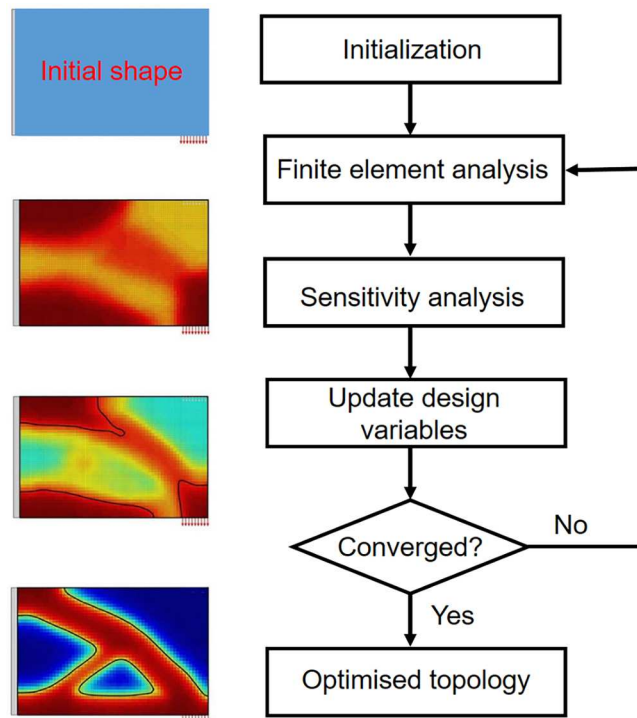
Figure 3. Flow chart of the topology optimisation procedure [35,47].

some design principles proposed for additive manufacturing components. For example, a digital design approach needs to be used to minimise material usage, improve functionality, and consolidate part assemblies. In addition, the design should be tailored for the correct additive manufacturing process.

(1) Cellular structures to minimise material usage and improve functionality. Lattice materials as illustrated in Figure 1 provide a promising way to minimise material usage with improved functionality. Transport properties often occur through porous lattice materials. With precise control of the lattice structure distributions via digital design, a maximum performance of the energy storage system can be achieved. The interconnected

porous phases are usually used to enhance transport properties. Take the TPMS structures as an example, results have demonstrated that the Schwartz P surface can achieve the maximal fluid permeability and electrical/thermal transport properties [32,48]. The electron and ionic transport kinetics can be significantly enhanced by using these lattice structures.

(2) Multi-physics modelling and inverse design. There are complex multi-physics transport mechanisms within energy storage systems. The fundamental equations of heat transfer or electrochemical need to be used to guide the microstructure design to achieve the maximised performance. By combining multi-physics modelling with an inverse design strategy, rational engineering
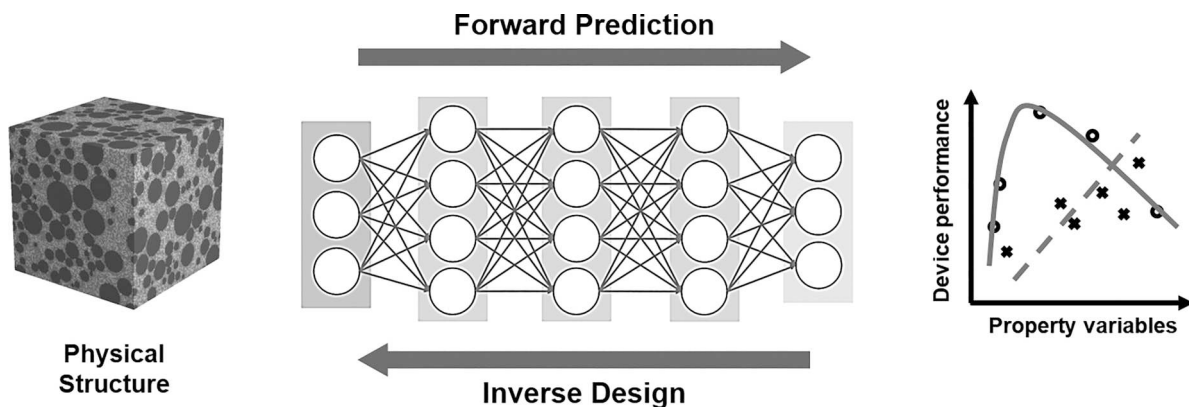
Figure 4. Framework of the data-driven design approach.

of structural materials in energy storage systems can be achieved.

(3) Structure design for the proper fabrication process. Integration of the structure design with the proper AM process is important. For instance, topology optimisation is commonly used to generate structures with optimised performance. Unique structures need to be tailored to be successfully fabricated with suitable support structures/templates. Depending on specific AM processes, anisotropic functionalities, and support structures need to be optimised via a digital design approach [49,50]. On the other hand, each AM technique has suitable material types, e.g. high-conductive metal materials and insulating polymers. DIW is commonly used to fabricate electrochemical energy storage devices and thermal energy storage composites. The fabrication process (e.g. extrusion speed, material viscosity) will significantly affect the final product quality.

As high value-added material is commonly used in energy storage systems, the usage of lattice structure's digital design principles is also highly relevant to cost reduction. Design principles can be incorporated with economic evaluation to guide realistic fabrication processes.

3. Additive manufacturing technique

Additive manufacturing, commonly known as 3D printing, is an umbrella term used to describe a range of technologies that construct digitised structures layer-by-layer, using designs by computer-aided design software [51]. In contrast to conventional subtractive manufacturing, the AM can produce high-quality customisable components from ceramics, metals, and polymers without additional costs of machining or moulds [52]. It is clear from previous research works that AM offers significant potential to accelerate the creation of novel and complicated designs as well as to advance the research of energy conversion and storage applications [51]. In the following, six widely used AM techniques: vat photopolymerization, powder bed fusion (PBF), material jetting, binder jetting, material extrusion, as well as directed energy deposition (DED) are discussed. Schematics, materials, brief descriptions, and limitations are presented in Table 2.

3.1. Vat photopolymerization

Vat photopolymerization builds a 3D object by solidifying a vat of photopolymer resin layer-by-layer [53]. Stereolithography (SLA) is the earliest vat photopolymerization technology. The liquid photosensitive resin surfaces are scanned by lasers with specific wavelengths and intensities for polymerisation. Sequential solidification is realised from point to line, and then from line to surface. When the mapping operation of one level is completed, the platform is raised one layer's height vertically to cure another level. The layers are stacked in this way to form a 3D entity.

The digital light process (DLP), using a projector instead of a laser to expose the entire layer of resin, operates on a similar premise to SLA. DLP printing is quicker than SLA since it does not require point-by-point scanning.

Continuous liquid interface production (CLIP) enables fast printing, which continuously pulls up the model and keeps moulding. CLIP requires a low-viscosity resin and a hollow model, which ensures fast resin replenishment to the print area and reduces the amount of resin required per layer.

In general, vat photopolymerization processes can be applied to produce parts with high-quality surface, making them suitable for jewellery, investment casting, dental and medical applications. The major disadvantages include the lack of mechanical strength and the limitation of print size as well as materials that need to be photocurable [54].
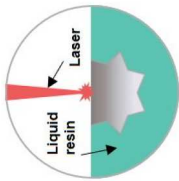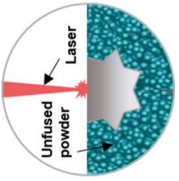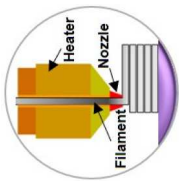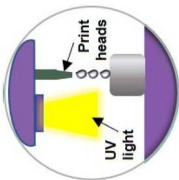
3.2. Powder bed fusion

PBF is an AM technique in which powder material layers are selectively fused or melted by a heat source (a laser or electron beam) to create solid 3D objects.

For the selective laser sintering (SLS) process, powders are spread on the upper surface of the formed part and scraped flat. A high intensity carbon dioxide laser is utilised to scan the cross-section over the freshly laid new layer. To create the new cross-section and bond it to the formed part below, the powdered material is sintered together under the high intensity laser light. The build platform is lowered to another height once one sintered layer is finished, and new powder material is subsequently laid on the surface.

SLM and direct metal laser sintering (DMLS) processes can fabricate components in the same way as SLS, except that both techniques are employed to manufacture metal parts and typically require the addition of supports to resist residual stresses in the manufacturing process. Specifically, SLM is applied to fabricate pure metals, while DMLS is aimed at alloy parts. At present, DMLS is broadly utilised to manufacture highly stressed components and complex or irregular components that cannot be handled by traditional machining technologies. It can achieve 90% to 95% of the highest strength of the same grade metal. With high precision and

Table 2. Categories of additive manufacturing technologies.

Categories	Vat photopolymerization	Powder bed fusion	Material extrusion	Material jetting	Binder jetting	Directed energy deposition
Schematics						
Brief description	Liquid photopolymer in a vat selectively cured by light-activated polymerisation	Powder bed areas selectively fused by thermal energy	Material selectively dispensed through an aperture or nozzle	Selective deposition of build-material droplets	Selective application of a liquid binder to bond powder materials	Materials fused by melting during deposition using focused thermal energy
Technologies	SLA, DLP, CLIP	SLS, SLM, DMLS, EBM	FDM, FFF, DIW	EHD, AJ, PolyJet, MJP	MJF, SPJ	LENS, EBAM, LDW
Feedstock	Liquid	Powder	Filament, rod, liquid	Liquid	Powder, liquid	Wire, powder
Materials	Photopolymers	Metal, polymers	Thermoplastics, metal, concrete, viscoelastic liquid	Photopolymers, metal, wax	Metal, polymers (ABS, PA, PC), ceramics	Metal, alloys
Bonding and join	Cured with laser, projector, UV light	Fused with laser and electron beam	Fused with heat, adhesive force	Cured with UV light, heat	Jointed by adhesive binder	Fused with laser, electron beam, plasma-arc or electric-arc
Applications	• Fine details • Smooth surface finishes • Jewellery • Medical applications	• Functional metal (aerospace and automotive) • Energy systems • Medical treatment • Dental care	• Functional engineering prototypes and systems	• Prototyping and tooling (full-colour) • Medical models • Moulds and casting patterns production in small batches • Electronic devices	• Functional metal parts • Full-colour model • Sand casting	• Repairing and remanufacturing automotive and aerospace components
Benefits	• Smooth surface • Fine details	• Strong parts • Scalable (fits size) • Complicated geometry • No support	• Fast • Low cost • Common thermoplastics	• Excellent details • High accuracy • Realistic prototypes • Smooth surface	• Full-colour options • A variety of materials • No warping or shrinking • No support	• Strong parts • Range of materials • Larger parts
Limitations	• Brittle • UV sensitive • Usually require supports • Extensive post processing	• Longer production time • Higher cost (Machinery, material, operation)	• Rough surface finish • Anisotropic • Usually require supports • Not scalable • Limited accuracy	• High cost • Anisotropic mechanical properties	• Low part strength • Lower accuracy than material jetting	• High cost • Poor surface finish
References	[63]	[64]	[30,65]	[66]	[67]	[68,69]

minimal moulding restrictions, DMLS is widely used in high-end precision manufacturing.

Electron beam melting (EBM), an AM technique that closely resembles SLS, utilises a high-energy electron beam rather than a laser to fuse the metal powder. EBM generates less residual stress within a printed part, thus causing less distortion and requiring fewer support structures. The EBM process not only consumes less energy, but also is more efficient than the SLS process, with increased layer thickness, minimum feature size, powder size, and surface roughness. Compared with SLS, electrically conductivity and vacuum environments are necessary.

The PBF process enables functional part fabrication with complex geometry and high strength for energy systems. The main shortcomings of the PBF process are poor surface quality (e.g. surface roughness and porosity), slow production rate, part shrinkage, and relatively high cost [54].

3.3. Material jetting

Material jetting is an inkjet printing technique that utilises print heads to deposit liquid photoreactive material droplets layer by layer onto a cured plate. Similar to SLA, the deposited material is then exposed to ultraviolet (UV) light, which cures the layer of material through a photopolymerisation process. The two mainstream material jetting processes include aerosol jet (AJ) printing and electrohydrodynamic (EHD) jet printing [55]. A continuous or drop-on-demand (DOD) jetting approach can be used for the material deposition strategy. Specifically, viscous liquid materials are usually deposited using the DOD technique [56].

The materials used in material jetting involve photopolymers (in liquid form) and casting wax. Substantial research is underway to extend the scope of materials that can be utilised via material jetting. Ceramics, metals, and silicones have begun to enter the market. For metals and ceramics, the Israeli company Xjet, for instance, developed its NanoParticle Jetting technique [57]. Silicone 3D printing, developed by ACEO, has made another material advancement for material jetting. The ACEO technology was first unveiled in 2016 and used a 'drop-on-demand' technique to produce parts made entirely of silicone or multiple materials in a range of colours and hardness [58].

Among AM techniques, material jetting boasts one of the highest accuracy levels. In light of the precise deposition of the tiny droplets, layers can be printed as slight as 0.013 mm, providing a magnificent degree of detail, high precision, and smooth surface completion. Material jetting may be applied for full-colour and multi-material

3D printing since the print head utilised in the printing process often processes multiple nozzles. Additionally, support structures can be easily dissolved in an ultrasonic bath without surface damage after removal. The drawbacks of material jetting mainly involve high cost, slow printing process, and poor mechanical properties, especially in contrast with other AM techniques such as SLS, which render material jetted parts usually inappropriate for functional applications.

3.4. Binder jetting

Binder jetting involves applying a liquid binder to the powder bed one layer at a time, selectively bonding areas of the powder bed to make a solid component. In contrast to other AM processes, binder jetting does not require heat. Construction materials are held together by an adhesive binder. While the powder material is employed to make up the majority of the overall object mass, the print head only deposits trace amounts of the binding ingredient. Post-processing is normally required to strengthen the part and enhance the mechanical and structural characteristics of the binder material [53]. Afterwards, the object is taken out of the powder bed, and compressed air is applied to remove any unbound powder.

Metal, polymers, and ceramics are commonly used as powder materials in the binder jetting process. Multi jet fusion (MJF) and single pass jetting (SPJ) are two commercialised binder jetting techniques [59,60]. The process is usually faster than others and may be further accelerated by adding more print heads. By varying the ratio and individual characteristics, a wide range of distinct binder-powder combinations and mechanical characteristics of the final model are produced. This process is therefore appropriate when the internal material structure must meet a certain quality standard.

The binder jetting process enables fabricated parts with varied colours and materials. Binder jetting is utilised in various applications, including full-colour prototypes (such as figurines), inexpensive metal parts, as well as large-scale sand-casting cores and moulds. However, the binder jetting process is not always appropriate for structural parts owing to its low mechanical strength.

3.5. Material extrusion

Material extrusion fabricates 3D structures by extruding filaments through a nozzle, melting the materials, and depositing them layer by layer onto a substrate. Typical material extrusion techniques include fused deposition modelling (FDM), direct ink writing (DIW), and fused filament fabrication (FFF).

FDM is a non-laser filament extrusion process where engineering thermoplastics are heated from filaments and extruded in layers to construct the part. It is the most common material extrusion technique [52]. The materials used for FDM are relatively inexpensive, and there is no risk of toxic gas and chemical contamination. However, further polishing is required due to the rough surfaces of fabricated parts. The FDM technology, which aims to produce 3D printed parts at a low cost, may also produce metal parts [8,9].

DIW has been extensively implemented to produce micro-scale energy devices, particularly in the electrochemical energy storage field [18]. To fabricate 3D architectures with a micrometre-scale resolution, viscoelastic liquid material is extruded through a nozzle tip. The extrusion techniques include piston extrusion, pneumatic extrusion, and screw extrusion. It offers a versatile way to print various materials, ranging from biomaterials to ceramics.

In comparison to other AM techniques, the material expenses utilised in material extrusion processes as well as the extrusion moulding are comparatively low, and a wider range of materials are accessible. However, the fabricated parts cannot achieve the same mechanical properties as forged metals. The unpredictable shrinkage restricts its utilisation for large-size parts [52].

3.6. Directed energy deposition

DED is a metal AM process where wires or powders are fused by melting as they are deposited on the substrate using focused thermal energy (e.g. electron beam, laser, electric-arc, or plasma-arc). DED systems include various types of machines utilising laser beam, electron beam, electric arc, or plasma arc energy sources. Typically, the feedstock is made up of either powder or wire [61]. Deposition normally takes place in inert gas (laser beam systems or arc systems) or vacuum (electron beam systems). The laser engineered net shaping (LENS) technique, laser deposition welding (LDW), and electron beam additive manufacturing (EBAM) are DED techniques that have been commercialised [62].

DED technique is used specifically for metal AM and is compatible with a versatile set of metals such as stainless steel, titanium, copper, aluminium, as well as alloys. Due to the material's adaptability, DED has a range of applications and can produce products in numerous industries. They are excellent for refinishing or incorporating material into already-existing parts such as turbine blades. However, the reliance on dense supporting structures of DED indicates the unsuitability of manufacturing parts from scratch.

The advantages of DED over other metal AM techniques include higher deposition rates and the capability to produce larger parts. DED is usually employed in the production of low volume parts, rapid prototyping, and repairs. Nevertheless, the main problems are residual stresses, rough finishing surfaces, and high equipment expenses [54].

3.7. Summary

Among the above-mentioned AM techniques, material extrusion and material jetting are commonly used for electrochemical energy storage devices and electronics [70]. The material extrusion and material jetting approach have the advantages to precisely deposit functional inks. Various functional materials have been developed (e.g. conductive polymers, carbon nanomaterials) with improved electrical and mechanical properties [70]. This offers an opportunity to fabricate highly innovative and customised electrochemical energy storage devices. For the thermal energy storage systems, SLM techniques have been used to fabricate the performance enhancement structures, e.g. fin configurations [12], and lattice structures [71]. As the thermal storage system performance is heavily dependent on device geometry and material properties, composite phase change materials (PCMs) were fabricated by AM techniques such as SLA, SLS, FFF, and DIW [17]. As matrix materials to enhance PCM thermal properties, filament, ink, resin, or powder material were developed and incorporated into different AM techniques. In most cases, each AM technique can only be used for specific purposes. As AM technique advances, it is expected it will play a more important role in the energy storage field.

4. Applications of AM for energy storage devices

Applications of AM in electrochemical and thermal energy storage systems are reviewed. There are some similarities in these two systems: (1) the system performance is heavily dependent on the transport mechanisms that could be understood via multi-physics modelling. In electrochemical energy storage systems, electron transport is driven by voltage potential while hindered by an electrical resistance. In thermal energy storage systems, thermal conduction needs to be enhanced to improve system performance [72]. (2) in these systems rationale design of 3D structures (e.g. pore distributions in battery electrodes, fin configurations in thermal energy devices) to enhance transport properties is important. (3) active materials with optimised microstructures and compositions are suitable to be fabricated via AM.

4.1. Electro-chemical energy storage

In this section, the applications of AM in different electrochemical systems, e.g. batteries, fuel cells, and supercapacitors are reviewed. These systems possess distinct energy storage and conversion mechanisms, but they all have electrochemical features to achieve high energy and power density. It is worth mentioning that various parameters need to be considered to achieve the best electrochemical performance, e.g. intrinsic material properties, and component interface. In this work, we focus on controllable microstructures and additive manufacturing. Well-designed shapes and internal structures can lead to improved performance. The 3D porous structures can improve electron and ionic transport properties as they provide highly accessible active surfaces and diffusion pathways. Further, the electrochemical performance can be predicted by digitally controlling the composition distribution and porosities [73].

4.1.1. Lithium-ion batteries

Lithium-ion batteries consist of four key components: cathode, anode, separator/electrolyte, and current collectors. Traditionally, the battery electrode is manufactured by coating the slurry on the current collector with a controlled thickness (∼100 μm). By using AM, 3D electrode microstructures could be fabricated with improved battery performance. The 3D structures can provide shorter diffusion lengths and smaller transport resistance, enabling increased energy density within a limited available space. Additive manufacturing has been used to print various kinds of batteries, e.g. lithium-ion battery [74], sodium-ion battery [75], and zinc-silver battery [76]. In the following, lithium-ion batteries with architectured electrodes are mainly reviewed.

For manufacturing lithium-ion batteries, AM can be used to deposit electrochemically active materials with desired architectures. Table 3 presents a summary of additive manufactured batteries by various techniques and design approaches, e.g. laser, lithography, electrode deposition, and extrusion. DIW can be applicable for various materials using continuous extrusion of shear-thinning inks (Figure 5 (a)). The materials that have been printed include $LiFePO_4$ (LFP) [74], Li-Titanate (LTO) [77], sulphur composites [78], and graphene oxide [79]. Typically, to maintain the 3D structure shape, inks with high yield stress and mechanical strength are required. The printing resolution is within a range of 1–500 μm which is restricted by the nozzle size. Figure 5 (b) depicts the FDM technique to fabricate the battery electrodes. The conductive active materials are well mixed with thermoplastic materials to produce composite file pieces, and the 3D printing filaments are produced via an extruder. The 3D electrode structures are fabricated by extruding filaments through a heated nozzle [80]. DLP technique has been used to manufacture carbon and lithium cobalt oxide 3D structures [81,82]. As demonstrated in Figure 5 (c), the microstructure made of acrylate-based resin is firstly fabricated. Afterwards, the printed samples were pyrolysed under vacuum at 1000 °C. The 3D polymer architecture and the architected carbon after pyrolysis are illustrated in Figure 5 (c).

The most commonly used AM technique for lithium-ion battery manufacturing is DIW. This is possibly because FDM and DLP utilise insulating polymer materials, however high conductive composite materials are usually needed for the battery systems. As a novel, contactless AM technique, Aerosol Jet printing has recently been used in battery manufacturing [83–85]. Compared with the traditional AM approach, Aerosol Jet printing has advantages such as scalability, and compatibility with a range of materials.

Usually, the 3D printed batteries are assembled in a sandwiched or in-plane design (Table 3). The sandwich-type batteries are fabricated by stacking of layered cathode and anode. This type can be applied in large-scale energy storage applications and is cost-effective [18]. Hu et al. [86] developed 3D printed cathodes based on $LiMn_{1-x}Fe_xPO_4$ (LMFP) nanocrystal cathodes. Compared with the traditional electrode, the 3D printed electrode has a 108.45 mAh/g capacity at 100 C rate. The in-plane design has advantages such as enhanced ionic transport properties and high contact surface areas. The 3D printed in-plane batteries have demonstrated superior electrochemical performance. One pioneering work is conducted by Sun et al. [74]. As illustrated in Figure 5 (a), thin-walled anode and cathode structures utilising LFP and LTO viscoelastic inks were 3D printed and tested. As it can facilitate ion and electron transport, the 3D interdigitated battery architectures with a high aspect ratio (up to 11 for an as-prepared 16-layer electrode) show excellent areal energy and power density. Later, Fu et al. [77] investigated the application of graphite oxide (GO) inks and solid-state polymer electrolyte on the 3D printed multi-layered structure. The battery with the GO matrix had a high initial capacity of 91 mAh/g.

AM offers the possibility to fabricate the battery system with complex architectures. Several novel design strategies have been proposed by tailoring the configurations of battery electrodes, either experimentally or numerically [87]. The 3D configurations can be interdigitated [74], concentric [88], and periodic porous structures [89]. 3D continuously porous structures

Table 3. Examples of battery design and fabrication by AM.

Additive manufacturing technology	Anode/Cathode	Feature resolution	Design approach/unique properties	References
SLS	NCA	100 μm	The influence of process parameters on the sintering of NCA powders was investigated.	[94]
Lithography-based 3D printing	LiTiO$_2$/LFP	–	Thin film batteries were fabricated on 3D printed polymer substrates.	[95]
DLP	Li/LCO	100 μm	LCO cubic lattices were fabricated with a resolution of 100 μm.	[82]
DLP	Li/Li$_2$S-C	50 μm	Octet-truss lattice structured Li-S cathodes were fabricated.	[96]
DLP	Li/Pyrolytic carbon	25 μm	3D architected carbon electrodes were fabricated and tested.	[81]
SLA	(LTO/PEGDA)/(LFP/PEGDA)	30 μm	Gel polymer electrolyte was printed via stereolithography	[97]
DIW	LTO/LFP	30 μm	Interdigitated secondary architecture with different layers were printed and tested for the first time.	[74]
DIW	(LTO/GO)/(LFP/GO)	180 μm	Interdigitated secondary architecture with solid-state electrolyte inks.	[77]
DIW	Li/LMO	150 μm	The micro-/macro structures were controlled by an electric field and additive manufacturing.	[98]
DIW	Li/LFP	50 μm	A novel low-temperature 3D printing was compared with conventional direct ink writing and roller coating process	[99]
DIW	Li/LFP	200 μm	3D thick LFP electrodes with different thicknesses and lattice structures (circle-line, circle-ring, circle-grid,)	[89]
DIW	Li/(Sulfur copolymer/graphene)	200 μm	The 3D printed Li-S battery has a high reversible capacity of 812.8 mAh/g.	[78]
DIW	Li/(Sulfur/carbon)	150 μm	High sulfur-loading of 5.5 mg/cm^2 cathodes were printed with specific discharge capacities of 1009 mAh/g.	[100]
DIW	Li/(Sulfur/graphene/phenol formaldehyde)	150 μm	Wearable Li-S battery was printed with a capacity of 505.4 mAh/g.	[101]
DIW	LTO/LFP	50 μm	Fully 3D printed LIBs with an areal capacity of 4.45 mAh/cm^2.	[102]
DIW	LiF-Li-Mg/LFP	350 μm	3D printed lithium salt scaffolds as metal-based anodes.	[103]
DIW	Li/Si	150 μm	Porous Si scaffolds were manufactured by 3D printing and sintering.	[104]
DIW	Li/LiMn$_{0.21}$Fe$_{0.79}$PO$_4$	18 μm	3D lattice structure with controlled electrode pillar size to achieve ultrahigh rate and high capacity.	[86]
DIW	(CNF/Li)/(CNF/LFP)	150 μm	Cellulose nanofiber (CNF) was used to fabricate the lithium metal battery.	[105]
DIW	Li/(Ni/rGO)	200 μm	Ultrathick electrode for Li-CO$_2$ was designed and fabricated by 3D printing.	[106]
DIW	LTO/LFP	200 μm	Fibre-shaped LFP electrodes were fabricated for wearable energy storage.	[92]
DIW	Li/Li	12.5–125 μm	Solid electrolyte microstructures with different patterns (line, grid, and column) were 3D printed.	[107]
DIW	(LTO/CNF/PVDF)/(LFP/CNF/PVDF)	100 μm	3D printable Li-ion battery electrolytes.	[108]
DIW	Li/MnO$_2$	200 μm	Solid electrolyte fabrication with different microstructures, e.g. 3D radial array structure.	[109]
DIW	Li/hGO	250 μm	Lattice structures with hierarchicalporosities were fabricated.	[79]
DIW	LTO/LFP	200 μm	3D Printed electrodes with interconnected conductive network and hierarchical pores.	[110]
DIW	Li/NC-Co	200 μm	Hierarchically porous carbon framework in Li-O$_2$ batteries.	[111]
Multi-axis extrusion process	Li/LFP	2.5 mm	Cathode doped materials were extruded together with polymer electrolyte coated carbon fibers to fabricate the battery.	[112]
FDM	Li/(LTO/PLA) and Li/(LFP/PLA)	1.75 mm	Disc and spiral shaped electrodes were printed and tested.	[113]
FDM	(Graphite/PLA)/(LFP/PLA)	0.05 mm	Various infill densities and Hilbert curve patterns were printed and tested.	[114]
FDM	(LTO/PLA/graphite/MWNT)/(LFP/PLA/graphite/MWNT)	200 μm	A novel design of a multi-coaxial-cable battery was proposed.	[88]
FDM	(LTO/graphene/PLA)/(LMO/MWNT/PLA)	100 μm	Wearable electronic devices with batteries were fully printed.	[93]
FDM	Li/LCO and Li/LTO	0.1 mm	Full ceramic LTO anode and LCO cathode were printed.	[115]
FDM	(Graphene/PLA)/Li	0.25 mm	3D printable graphite/PLA filament for negative electrodes.	[80]
Material jetting	Li/LFP	7 μm	Aqueous LFP-based electrodes were fabricated	[116]

show unique properties as they can offer features such as rapid mass transport, open space, large electrode surface area, enhanced mechanical property, and tailorable electric/thermal conductivity, for which offer great promise for the energy storage device designs. The lithium-ion batteries with bi-continuous surfaces are illustrated in Figure 6. Researchers have attempted to tailor the pores at the nano-scale to synthesise the 3D continuously porous microstructures with improved battery performance [90]. Template-based methods are commonly used to fabricate these bi-continuous architectures. One pioneer work on the bi-continuous electrode was proposed by Zhang et al. [19] (Figure 6 (a)). As illustrated in Figure 6 (a), the preparation of self-
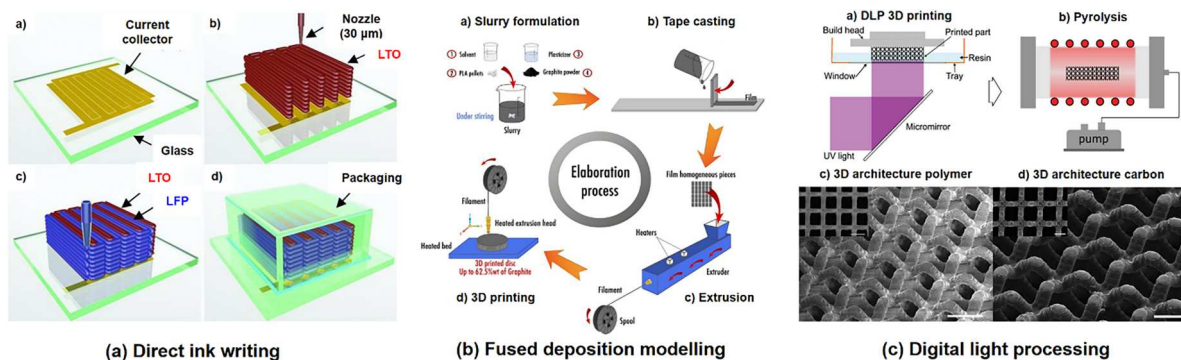
Figure 5. Additive manufacturing techniques for lithium-ion battery manufacturing: (a) Direct ink writing (DIW) [74] (b) Fused deposition modelling (FDM) [80] (c) Digital light processing (DLP) [81].

assembled opal templates was followed by the electro-deposition of a thin layer of nickel through the vacuum region. After removing the template, active materials were deposited on the nickel scaffold. The results showed that the rates of lithium-ion and nickel-metal hydride chemistries can reach up to 400 and 1000 C. The 3D templates in this work are not fabricated via conventional additive manufacturing techniques. However, it is a pioneer work to fabricate 3D patterned structures with enhanced electrochemical performance in reality. Using holographic lithography and conventional photolithography, Ning et al. [75] fabricated

high-performance Li-ion batteries with 3D periodic geometries (Figure 6 (c)). A SU-8 3D lattice was firstly produced on the indium tin oxide (ITO) coated glass surface. Afterward, photoresist AZ9260 was infiltrated into the 3D lattice to define the battery electrode pattern. Then, Ni was partially deposited onto the porous SU-8 lattice. By removing the photoresist template, a 3D porous Ni scaffold was obtained. Finally, active materials manganese dioxide (MnO_2) and nickel-tin (Ni-Sn) were further electroplated onto the surface as cathode and anode, respectively. The fabricated micro-battery has a high energy density (6.5 μWh/cm^2)
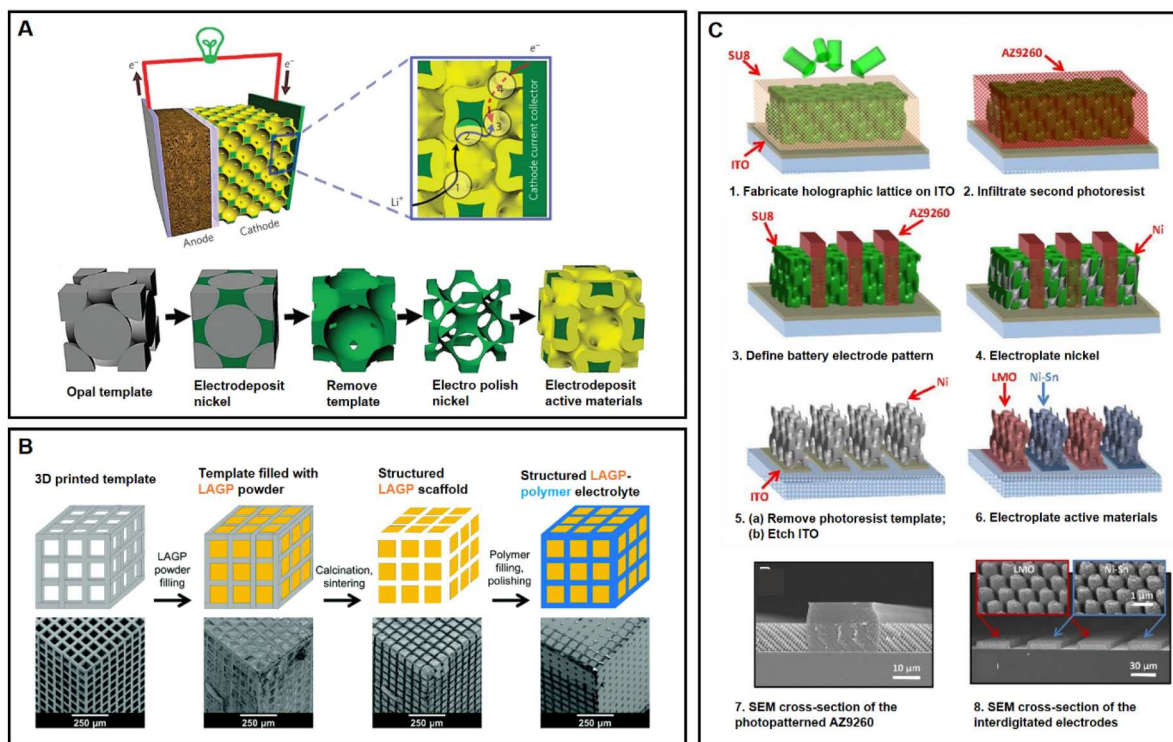
Figure 6. Fabrication of 3D structured lithium-ion batteries: (a) Illustration of a battery containing a bicontinuous cathode, and the electrode fabrication process [19] (b) 3D bicontinuous structured electrolyte [91] (c) 3D porous electrode fabricated by 3D holographic patterning technique [75].

and good capacity retention. The triply periodic minimal surfaces (TPMSs) show superior performances when used as battery electrodes [21,32], such as gyroid structure for high-energy lithium–sulfur (Li-S) batteries [22], and nano-gyroidal 3D interpenetrating solid-state electrochemical energy storage device [23]. Hybrid electrolytes made of 3D bicontinuous ceramic and polymer microchannels were reported by Zekoll et al. [91]. As shown in Figure 6 (b), cubic lattice structures were firstly fabricated using stereolithography 3D printing. The ceramic lithium-ion conductor powders were filled in the empty portions of the structure. Next, a structured $Li_{1.4}Al_{0.4}Ge_{1.6}(PO_4)_3$ (LAGP) scaffold was created by removing the polymer template and sintering the LAGP phase. An insulating polymer was filled in the original polymer space to form the hybrid electrolytes. The results show that the gyroidal architecture with epoxy polymer delivers the best performance with a total ionic conductivity of 1.6×10^{-4} S/cm.

The 3D printed lithium-ion battery can achieve 3D arbitrary shapes that can be integrated with printed electronics with mechanically flexibility. These advantages are beneficial for wearable electronics. Wang et al. [92] applied AM to fabricate a flexible all fibre lithium-ion battery. High storage modulus inks are used to fabricate the LFP and LTO electrodes that have excellent flexibility and electrochemical performance. The device has a specific capacity of 110 mAh/g, and can be incorporated into textile fabrics as wearable electronics. By using FFF 3D printing, a fully 3D printed wearable device with built-in 3D printed batteries was reported by Reyes et al. [93]. The polylactic acid (PLA) polymer was modified to have an ionic conductivity comparable to polymer electrolytes. Different material mixing ratios were investigated, and a maximum battery capacity can be realised when the active material to conductive material ratio is 20:80. By using 3D printing, portable electronic devices with integrated batteries could be fabricated in a single print.

4.1.2. Fuel cells
Fuel cells are devices that can convert chemical energy into power/electricity (Table 4). They offer benefits such as low expenses, high-power sustainability, and strong compactness. Traditionally, various ways have been used to fabricate fuel cell parts, e.g. dry pressing, casting, screen printing, and molding. These techniques are usually limited by poor resolution and weak mechanical properties, therefore are not suitable for complex configurations. AM provides a potential solution to address the above-mentioned challenges, especially to produce complex structures. It has been employed to fabricate various fuel cell components, e.g. solid oxide fuel cell (SOFC), protonic ceramic fuel cell (PCFC), and microbial fuel cell (MFC) [13].

Inkjet printing is one of the most widely used approaches to manufacturing fuel cells as it has a simple operation principle. By using inkjet printing, thin film electrolytes with a layer thickness less than 10 µm were fabricated (Figure 7 (b)) [117,118]. It offers the ability to uniformly distribute electrolyte materials, and fabricate dense and thin layers. Pham et al. [119] applied electrohydrodynamic jet printing to fabricate anode functional layer. With a 7–10 times thinner thickness, the electrohydrodynamic jet printed cell can achieve the same performance compared with the conventional way. Yu et al. [120] reported a porous thin film cathode fabricated using inkjet printing. The results show that ink-jet printed fuel cells exhibit reduced polarisation resistance when compared with conventional fuel cells. Inkjet printing is also applied to infiltrate catalysts into the porous electrodes. A scalable inkjet printing process was developed by Mitchell-Williams et al. [121] to infiltrate nanoparticles into SOFC anodes. The electrochemical performance can be improved. Using Inkjet printing, Wang et al. [122] fabricated porous $NiO-Gd_{0.1}Ce_{0.9}O_{2-x}$ scaffold, $Gd_{0.1}Ce_{0.9}O_{2-x}$ nanoparticles were then infiltrated into the pores, enabling the tailoring of micro-structured electrodes. Stereolithography is another commonly used slurry-based AM technique. Masciandaro et al. [123] printed the self-supported electrolytes with flat and honeycomb-like structures. The honeycomb-like electrolytes show enhanced performance with a power density of 115 mW/cm^2. In Arianna et al. work [124], planar and corrugated membranes were fabricated via stereolithography. By using the corrugated architecture with increased active area, the device exhibits a better performance with a power density of 410 mW cm^{-2}.

As shown in Figure 8, powder based 3D printing, e.g. SLS, is used to fabricate bipolar plates [125,126]. Guo et al. [125] investigated different graphite materials to fabricate bipolar plates. Optimised electrical conductivity of 120 S/cm and flexural strength of 40 MPa were achieved. The 3D printed bipolar plates were further tested in a single-cell and 40-cell stack by Gould et al. [126]. A constructal flow distributor was proposed by Ramos-Alvarado and Fan [127,128]. The number of branches was investigated. A series of bio-inspired flow field designs was proposed by Guo et al. [129]. As illustrated in Figure 8 (c), non-interdigitated and interdigitated configurations were investigated. By comparing with the conventional designs, the bio-inspired design shows a 20–25% higher peak power density than conventional designs.

**Table 4.** Examples of fuel cell design and fabrication by AM.

| Additive manufacturing technology	Fuel cell type	Feature resolution	Design approach/unique properties	References
SLS	Polymer electrolyte fuel cell (PEMFC)	101.6 μm	Graphite composite bipolar plates with desirable electrical and mechanical properties were fabricated.	[125]
DMLS	Solid oxide fuel cell (SOFC)	20–30 μm	Bipolar plates were fabricated for fuel cells, and the flatness needs to be improved in large stacks.	[126]
SLA	SOFC	250 μm layer thickness	Conventional planar structure (260 mW cm^{-2}) and corrugated structure (410 mW cm^{-2}).	[124]
SLA	SOFC	25 μm layer thickness	Flat and honeycomb-like membranes were fabricated.	[123]
DLP	SOFC	25 μm layer thickness	8 mol% yttria-stabilized zirconia ceramics were printed and tested with a power density of 114.3 mW cm^{-2}.	[130]
DLP	Microbial fuel cell MFC	500 μm pore size	A copper electrode with controllable pore sizes was fabricated. The power density is 12.3-fold higher than conventional electrodes.	[131]
DLP	SOFC	50 μm	Ripple-shaped electrolytes were fabricated, and a 32% performance improvement can be achieved.	[132]
Material jetting	SOFC	15 μm	Thin functional layers of electrolyte and anode were fabricated for SOFC.	[117]
Material jetting	SOFC	1.5 to 7.5 μm layer thickness	Thin-film electrolytes and buffering layers with precise thickness control.	[118]
Material jetting	SOFC	2.5 μm layer thickness	Porous silver film cathode with reduced polarisation resistance was fabricated by Inkjet printing.	[120]
Material jetting (Electromagnetically driven)	SOFC	–	Nanoparticles were infiltrated into SOFC anodes via inkjet printing.	[121]
Material jetting (Electromagnetically driven)	(SOFC)	–	The SOFC anode microstructure was tailored by inkjet printing infiltration, and a significant reduction of polarisation can be achieved.	[122]
Material jetting (Electro hydrodynamic jet)	SOFC	2–5 μm layer thickness	Grid-structured anode functional layers were fabricated with controllable printing parameters.	[119]
Material jetting	PEMFC	1200 Dots per inch	Catalyst materials of various shapes were deposited onto gas diffusion layers for PEMFCs.	[133]

4.1.3. Supercapacitors

The application of supercapacitors in micro-scale devices is gaining momentum in recent years [134]. Typical application areas include wearable electronics, remote environmental sensors, and nanorobotics. Compared with batteries, supercapacitors usually have higher power density, fast charge, and longer service life, enabling sustainable operation of self-powered micro/nanosystems [134].

AM offers the ability to manufacture capacitors with controlled pores and microstructures. Examples of supercapacitor fabrication via AM are listed in Table 5. Fully 3D printed supercapacitors were often achieved by extrusion-based direct ink writing (DIW). As illustrated in Figure 9 (a), water-based, printable MXene ink was used to manufacture the 3D printed micro supercapacitors with interdigital electrode architectures [135]. By using highly concentrated MXene ink with desired viscoelastic properties, multiple layers can be fabricated with improved areal capacitances (1035 mFcm^{-2} at 2 mVs^{-1} for ten-layer thickness). Azhari et al. [136] developed a powder bed additive
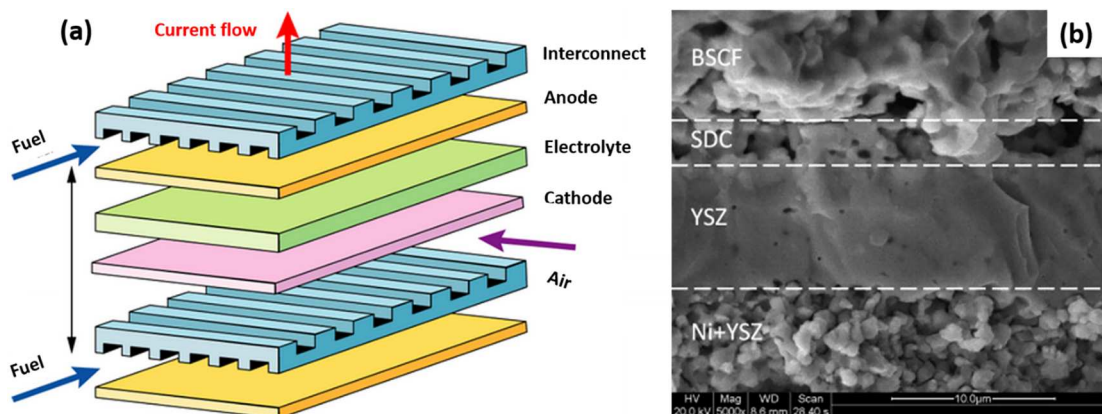
Figure 7. Illustration of a fuel cell stack: (a) Solid oxide fuel cell (b) Inkjet printing fabricated solid oxide fuel cell with a thin-film YSZ electrolyte, Ni+YSZ anode, SDC buffering layer, and BSCF cathode [118].
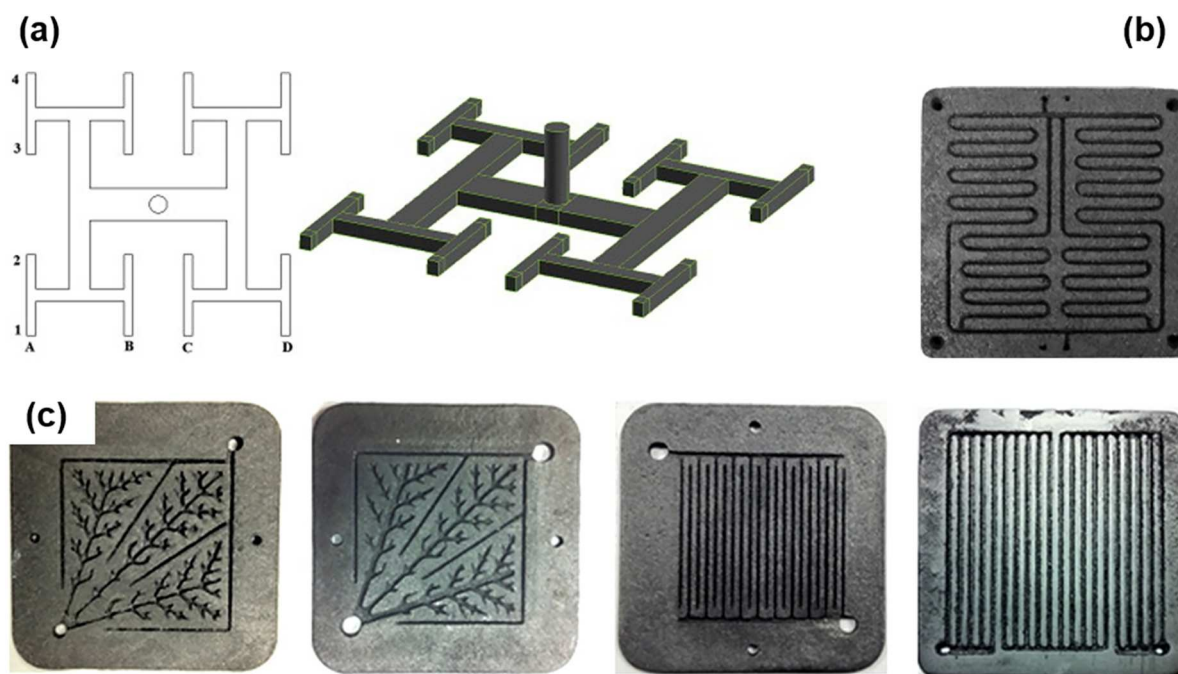
Figure 8. Fuel cell bipolar plate fabrication and design: (a) Constructal flow distributor [127] (b) Graphite bipolar plate with serpentine flow field [125] (c) Bio-inspired design and conventional interdigitated design [129].

manufacturing technique to fabricate millimetre thick graphene-based electrodes. As shown in Figure 9 (b), 3D structures of thermally reduced graphene oxide were fabricated by injecting an aqueous-based binder onto the powder bed. The fabricated electrode has a more porous microstructure compared with mechanically pressed electrodes. A novel hybrid additive manufacturing system was recently developed to fabricate electrochemical double layer capacitors (Figure 9 (c)) [137]. Low-cost filament fabrication and direct ink writing were combined together to fabricate supercapacitors in a single operation, offering a way to rapidly manufacture energy storage devices with irregular volume/shape.

Desired shapes of supercapacitors are controlled by computer aided design and fabricated by 3D printing, as demonstrated in Figure 10. By using a scalable, low-cost stamping strategy, MXene supercapacitors with interdigitated and spiral shapes were fabricated by Zhang et al. (Figure 10 (a)) [138]. In this work, 3D printed cylindrical and pad stamps coated with MXene ink were used to fabricate interdigitated structures. The $Ti_3C_2T_x$ supercapacitor can exhibit high areal capacitances (61 mF cm^{-2} at 25 μA cm^{-2} and 50 mF cm^{-2} at 800 μA cm^{-2}). A hybrid-dimensional electrode structure using interdigitated configurations was proposed by Tang et al. [139]. Using 2D graphene NSs and 1D silver nanowires as conductive additives, high device areal capacitance (412.3 mF cm^{-2} at 2 mA cm^{-2}) and energy density (65.4 μWh cm^{-2}) were achieved. The electron transport and ionic transport were significantly enhanced via the highly-conductive 3D network formed within the electrodes.

3D architectures have been used to further increase the energy density and reduce the electrolyte ion transport path. As shown in Figure 10 (b), 3D periodic graphene composite microlattices were fabricated by Zhu et al. [140] for supercapacitor applications. Graphene has unique properties of low density, high electrical conductivity, and thermal stability, and excellent mechanical characteristics [20]. With improved ion diffusion via ordered macropores, the 3D printed electrodes have exceptional capacitance retention and power densities. This work demonstrates the potential of AM to fabricate high mass loading scaffolds. A 3D design of interdigitated electrodes is illustrated in Figure 10 (c) [141]. In this work, 3D titanium interdigitated electrodes were fabricated based on SLM technology. Polypyrrole was deposited onto the electrode surface as an electroactive material. The fabricated device has an energy density of 213.5 Wh m^{-3} with a high capacitance retention after 500 and 1000 cycles.

Currently, most supercapacitor designs are based on 2D interdigitated configurations. These configurations don't need complex design principles. However, digital design approach can be applied to optimise the 3D micro lattices and interdigitated electrodes (Figure 10 b-c) to achieve the best performance.

Table 5. Examples of supercapacitor design and fabrication by AM.

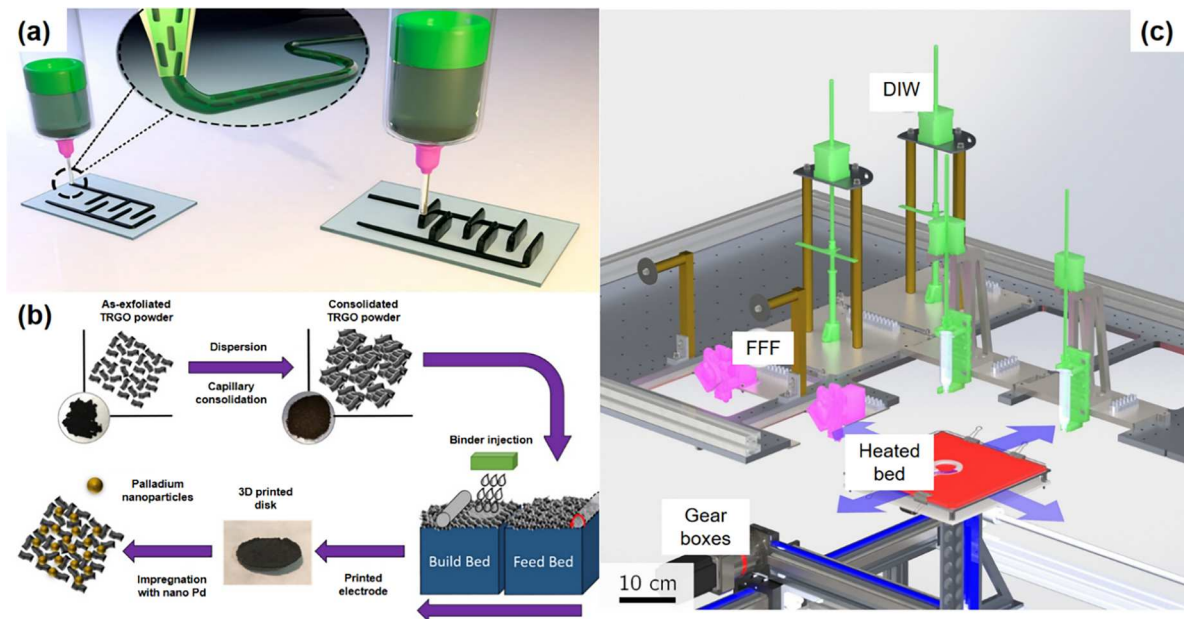| Additive manufacturing technology	Material	Feature resolution	Design approach/unique properties	References
SLS	Ti-6Al-4V metal powder for electrode fabrication	200 μm diameter pillar size	3D interdigitated supercapacitor with a volumetric capacitance of 2.4 F cm^{-3}, a power density of 15.0 kW m^{-3}, and an energy density of 213.5 Wh m^{-3} were produced.	[141]
Binder jetting	Graphene	100 μm	Electrodes with a thickness of 300 μm and an areal capacitance of 700 mF cm^{-2} were fabricated.	[136]
FDM	Activated carbon	–	Two printing systems were used to fabricate a double layer capacitor.	[142]
FFF & DIW	Activated carbon, electrolyte hydrogel	–	Double layer capacitors were fabricated by a hybrid-AM system in a single, automated operation.	[137]
DIW	Graphene oxide	21 μm	High-rate performance capacitors with 42.74 kW cm^{-3} power density and 4.43 mWh cm^{-3} energy density were fabricated.	[143]
DIW	Graphene oxide	20 μm	Planar interdigitated micro-supercapacitors were fabricated on flexible substrates.	[144]
DIW	Graphene	–	3D interdigitated supercapacitor for energy storage device in	[145]
DIW	Graphene aerogel	–	3D periodic graphene microlattices were fabricated for supercapacitor applications.	[140]
DIW	Carbon nanotube	–	A fully packaged integrated supercapacitor with high performance is fabricated.	[146]
DIW	Graphene	30 μm	Inkjet printing and dry etching are combined together to produce flexible and transparent micro-supercapacitors.	[147]
DIW	Graphene oxide	–	Ultrathick high energy density graphene oxide supercapacitors were fabricated.	[148]
DIW	Graphene oxide	500 μm	Supercapacitors with architectures e.g. hollow thin-wall columns, 3D honeycomb, and column lattice were fabricated and tested.	[149]
DIW	MXene	–	3D interdigital MXene electrode architecture with ultra-high energy densities was fabricated.	[135]
DIW	Graphene	–	An interdigitated graphene framework with a capacity up to 220.2 Cg^{-1} was fabricated.	[150]
DIW	Graphene	–	3D printed interdigitated supercapacitors with high areal capacitance (412.3 mFcm^{-2} at 2 mA cm^{-2}) and energy density (65.4 μWh cm^{-2}).	[139]
DIW	MXene	–	2D screen printing and 3D extrusion printing were used to print high energy density supercapacitors.	[151]
DIW	Graphene aerogel/MnO$_2$	0.24 mm layer thickness	A mm-thick 3D graphite aerogel/MnO$_2$ scaffold with linear increased areal capacitance is fabricated.	[152]
DIW	Activated carbon	100 μm	Porous carbon derived from packaging waste is used to fabricate solid-state supercapacitors.	[153]
DIW	Graphene aerogel	400 μm	Surface-functionalized graphene aerogel structure was fabricated.	[154]
DIW	Graphene aerogel	–	Inkjet-printed graphene interdigitated electrodes for supercapacitors and Na-O$_2$ batteries.	[155]
DIW	Graphene/conductive carbon	30 μm	Fully 3D printed solid-state micro-supercapacitors with Ni metallic current collector, electrode, and electrolyte layers.	[156]

4.2. Thermal energy storage

In this section, the applications of AM in thermal energy storage systems are reviewed (Table 6). Application of AM techniques for thermal energy conversion devices has been discussed in some review articles [157,158]. They offer benefits such as affordability, excellent thermal performances, and strong compactness. Compared with energy conversion devices, thermal energy storage devices heat or cool a medium to use the energy when needed later. For the latent heat thermal energy storage device, one main barrier is the limited thermal conductivity of molten salt media [159]. AM presents a potential solution to this problem, especially when it comes to creating materials with intricate structures. It has been employed in a variety of enhancement techniques, e.g. optimised fins with various extended surface configurations, impregnation of high thermal conductivity porous matrix, and form-stable composite PCMs. As these performance enhancement structures are commonly fabricated by different AM techniques, in the following subsections we discussed the applications according to different enhancement technology types.

4.2.1. Additive manufactured fins and extended surfaces

Using fins or extended surfaces has been proved to be an effective strategy for performance improvement. In a shell and tube configuration, the inner tube surface serves as a heat transfer surface and the PCMs are often placed in the annular space between the shell and tubes. During a charging process, heat is transferred from heat transfer fluid (HTF) to PCMs through the heat transfer surface. Heat transfer at the PCM phase is primarily controlled by conduction and convection. The heat transfer rate is higher and more phase transitions occur in the upper region of the device due to the density difference between the solid and liquid phases.

Figure 9. Additive manufacturing techniques for supercapacitor manufacturing: (a) Direct ink writing (DIW) of micro-supercapacitors (MSCs) with interdigital architectures [135] (b) Binder-jetting powder bed AM of thick graphene-based electrodes [136] (c) Hybrid additive manufacturing [137].

The presence of fins or extended surfaces can both improve the thermal conductivity as well as promote natural convection. During a discharging process, the liquid PCM near the heat transfer surface firstly releases the heat and forms a layer of solid phase, which causes additional thermal resistance between the HTF and unsolidified liquid PCM. Extended surfaces or fins can provide additional heat transfer and enable better contact between the liquid PCM and heat transfer surface. Among the various fin shapes, the longitudinal
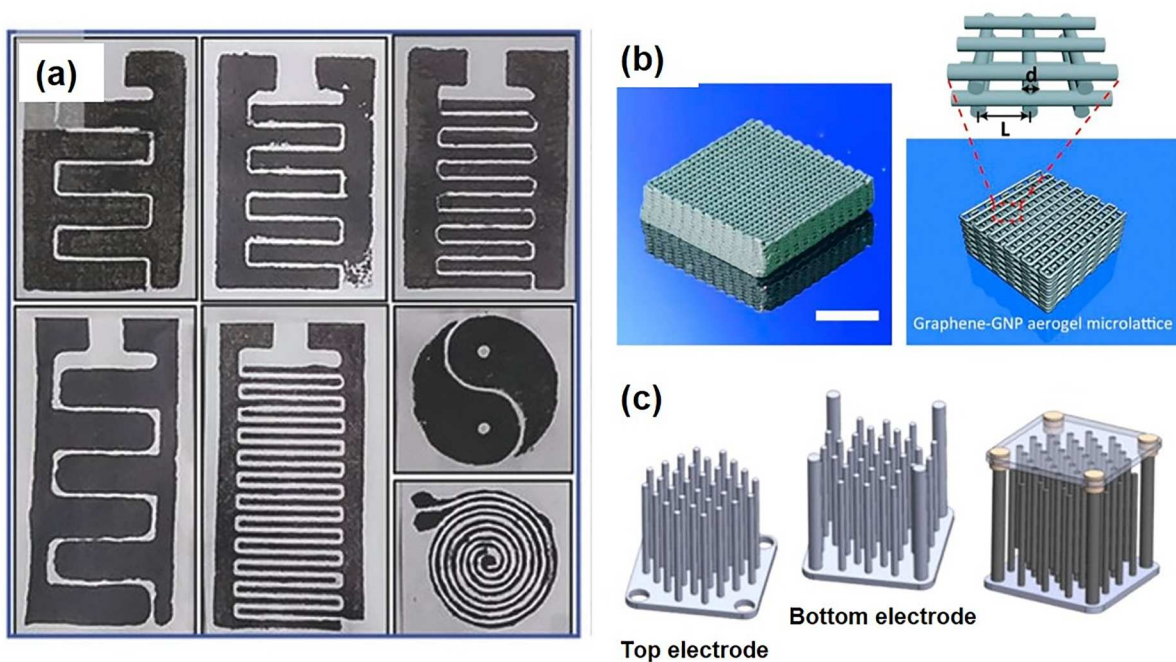
Figure 10. Additive manufacturing of supercapacitors: (a) Stamped MXene supercapacitors with various architectures [138] (b) Compressible graphene aerogel micro lattices fabricated by direct ink writing [140] (c) 3D interdigitated electrodes [141].

Table 6. Examples of thermal energy storage and fabrication by AM.

| Additive manufacturing technology	Dimension	Design approach	Remarks	References
SLM	Length: 185 mm External Diameter: 90 mm Thickness: 6 mm	Topology optimisation	The first AM multi-tube energy storage device	[12,160]
SLM	*Length* x *Width* x *Height*: 27 mm x 40 mm x 130 mm	Graded cellular structure	Phase-change temperature control with graded cellular design and thickness adjustment of the packaging structure	[26]
SLM	100 mm x 100 mm x 40 mm with a cell size of 10 mm	3D periodic cellular structures	Aluminum body-centred cubic cellular structures were fabricated and tested.	[27]
SLM	40 mm x 40 mm x 40 mm Porosity: 90%	Porous periodic cubic cell structure	Composite PCM embedded with a porous aluminium structure is fabricated.	[28]
SLM	Cell base: 10, 20, 40 mm Height: 40 mm Porosity: 95%	3D periodic structures	Fabrication of three different aluminum 3D periodic structures with enhanced heat transfer in the PCM heat storage	[162]
SLM	26 mm x 26 mm x 26 mm with cell sizes of 4, 6.5, and 9 mm	Lattice structures with TPMS structures	AM lattices are inserted into PCMs for heat transfer augmentation	[165]
DMLS	27 mm x 40 mm x 130 mm rectangular acrylic container	Lattice structures with internal and external fins	Enhanced thermal energy storage systems with AM technology	[71]
SLS	Diameter: 12.7 mm Thicknesses: 2–3 mm	Square, hollow square, and star structures	Expanded graphite/ paraffin wax phase change composite is made up by SLS	[168,169]
SLA	–	Topology optimisation	Optimal fin configurations in multi-tube LHTES systems with different PCMs	[16]
SLA	Pore dimensions (Ø3.2 mm; Ø6.4 mm)	Reticular structure	The bio-based PCMs integrated into a metallic structure made of copper and aluminum	[163]
SLA	4.5 cm x 3.5 cm x 0.25 mm	–	3D printable phase-change polysiloxane networks were developed for human body temperature management.	[166,176]
FDM	1.75-mm diameter Layer height: 0.2 mm	–	3D printable TPU blends with thermal energy storage capabilities	[170]
FDM	0.8-mm diameter Layer height: 0.4 mm	Miniaturized complex geometries	Microencapsulated PCM for thermal energy storage	[172]
FDM	1.75 mm diameter filaments	–	Phase change fabrics were 3D printed for multifunctional clothing.	[175]
FFF	25 mm diameter and 4 mm thick	–	Fused filament fabrication of novel PCM functional composites	[171]
DIW	0.6 mm layer height	–	3D printed polymer- PCM phase change material composites for thermal energy regulation	[173]
DIW	80–500 µm resolution	2D/3D complex patterns	PCMs were 3D printed as electronic packaging materials	[174]

and annular configurations are the most prevalent forms. The subsequent discussion will focus on how these types of fins are manufactured and employed to enhance the device's performance using AM techniques.

A high power density thermal energy storage device based on PCM was investigated by Moon *et al*. [71] (Figure 11 (a)). Internal and external fins to enhance heat transfer from the liquid coolant to the PCM were studied. Theoretical results show that the AM metal structures reduce conduction thermal resistance by 17 times and convection thermal resistance by 3 times compared to conventional designs. Three devices were made of an aluminium silicon alloy ($AlSi_{10}Mg$) and tested with paraffin PCM. Power density was measured to be 4 times better than traditional designs (0.58 W/cm^3).

Optimised fin configurations in multi-tube LHTES systems with different PCMs, flow arrangements, and design constraints were investigated by Pizzolato *et al*. [16]. The results show that realistic operating conditions need to be taken into account during the optimisation process. Additionally, the fin material should be chosen in parallel with the fin layouts. This indicates that the optimisation of latent heat thermal energy storage (LHTES) systems is a co-design challenge. As illustrated in Figure 11 (b), for the first time the additive manufacturability of topology-optimised LHTES units was demonstrated.

A shell-and-tube energy storage system with topology-optimised fins for the solidification process was investigated by Ge *et al*. [12]. SLM technology was used to fabricate the topology optimised fin configurations. The thermal performance is assessed and compared with that of a conventional square fin design by computational fluid dynamics (CFD). The results show that the solidification time of the topology optimised fin is significantly reduced by 57.1%. Later, Ge *et al*. [160] quantitatively analysed the thermal enhancement performance and economic efficiency of the shell-and-tube energy storage system (Figure 11 (c)). The results show that the optimised fins can achieve the best thermal enhancement performance, but can only be a
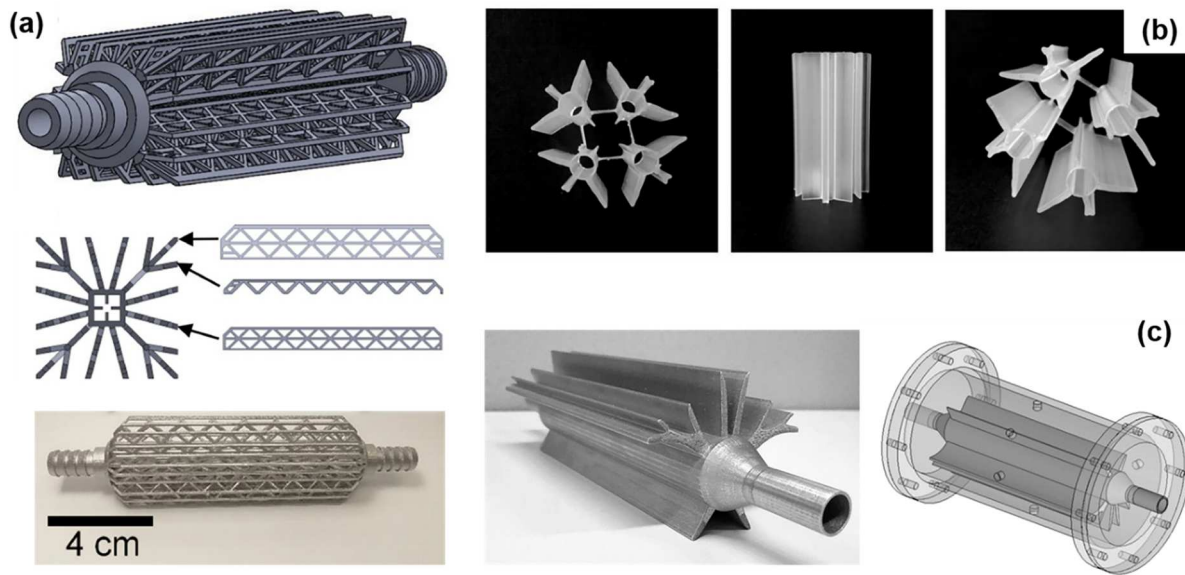
Figure 11. Additive manufactured fins and extended surfaces: (a) Additive manufactured device with external and internal fins to enhance heat transfer [71] (b) Additive manufactured multi-tube device with an optimised fin configuration [16] (c) Additive manufactured optimised fin configuration for melting performance enhancement [160].

cost-effective solution when the unit price ratio between the enhancement technique and the PCMs is less than 6. In future, it is necessary to focus on the design principles and the appropriate process parameters for additive manufacturing.

4.2.2. Impregnation of additive manufactured lattice structures

Impregnation of porous metal foams into the PCM was proved to be an effective method to improve the TES device efficiency [161]. The insertion of AM lattices with controllable structures into PCMs has gained increasing attention. Applications are shown in Figure 12. In contrast with conventional stochastic metal foams, the AM lattice porous structures with high mechanical and thermal properties have great potential in TES systems.

Zhang et al. [26] numerically analysed the integrated phase change temperature controller that simultaneously contained internal graded cellular material and external packaging structure fabricated by the SLM technique (Figure 12 (a)). Results show that the porosity distribution of the cellular materials and the wall thickness of the packaging structure have a significant influence on the performance. The heat transfer performance of thermal controllers can be improved by the collaborative design of the internal cellular materials and external packaging structures.

The melting of PCMs inside additive manufactured cellular periodic aluminium structures was investigated by Diani et al. [27]. As shown in Figure 12 (b), the

device is composed of periodic body-centred cubic cellular structures with 87% porosity. Three heat fluxes (10, 15, and 20 kW/m^{-2}) were considered for electronics cooling. Results indicate that melting the PCM takes a shorter time for finer metal structures.

Hu et al. [28] inserted a porous aluminum structure with cubic cells in paraffin (Figure 12 (c)). Both experimental and numerical results demonstrate that the total melting time is reduced by 38% compared to pure paraffin when using a porous metal structure (PMS). The temperature field of paraffin with PMS is more uniform, e.g. the maximum temperature difference can be decreased by about 81%. In addition, it is found that the energy storage rate is improved 1.2 times by using PMS. In the melting process, heat conduction plays an important role for the PCM with PMS whereas the pure paraffin melting is dominated by natural convection. Finally, it is found that high thermal conductivity PMS can drastically strengthen the thermal behaviour of PCM. The maximum enhancement ratio of PCM using a porous copper structure can reach 63%.

Righetti et al. [162] studied a novel LHTES system, consisting of PCMs embedded inside three distinct aluminum 3D periodic structures, with cell base sizes of 10, 20, and 40 mm and a porosity of 95%. Experimental results showed that the 3D structures process lower charging (up to 17%) and discharging (up to 38%) time. Moreover, the 10 mm base size structure has lower charging time, more homogeneous temperature distribution, and lower junction temperature than other samples relating.
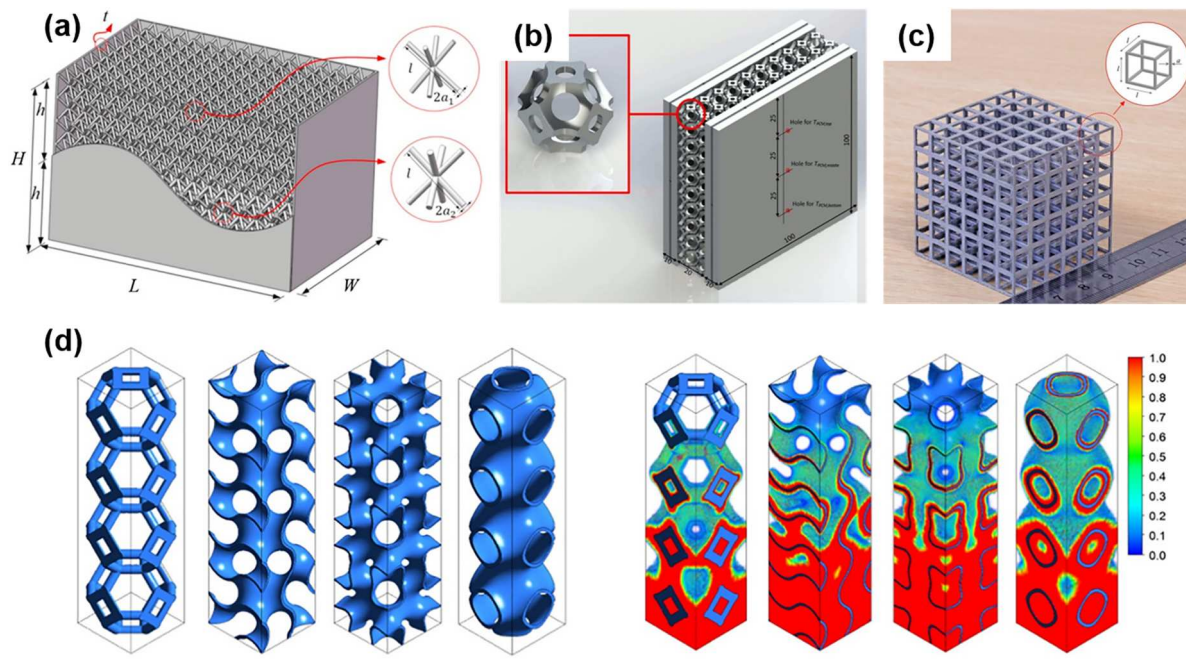
Figure 12. Impregnation of additive manufactured lattice structures: (a) Graded cellular design as thermal conductivity enhancer [26] (b) Periodic body-centred cubic cellular structures [27] (c) Periodic simple cubic cellular structures [28] (d) TPMS metal foam structures [29].

Almonti *et al*. [163] utilised bio-based PCMs derived from agricultural wastes. Since each material stems from biological wastes has a varied latent heat and melting/solidification point, this research considered the diverse thermal properties of the chosen material. Specifically, two aluminum and two copper alloy structures with distinct pore dimensions were fabricated by stereolithography technique. Four PCMs (Pure Temp 68, Crodatherm 60, Crodatherm 74, and Crodatherm ME29P) were melted and filled in the reticular structures, for a total of 16 combinations of integrated structures. The results demonstrated a 10% improvement in thermal storage/release for the copper reticular structure.

Recently, TPMS structures have gained attention in different areas. TPMS-based metal foam PCMs were numerically investigated by Qureshi *et al*. [29]. As shown in Figure 12 (d), three TPMS cells, namely Gyroid, IWP, and Primitive, were considered. By comparing with the Kelvin-based foams, the melting time can be reduced by 31%, 40.3%, and 35.3% for the Gyroid, IWP and Primitive-based PCMs. Later, they investigated the effect of lattice porosity and functional grading [164]. Zhang *et al*. [165] designed nine lattices with diverse cell types (GR-gyroid rod, WR-IWP rod, and GS-gyroid sheet), cell sizes (4, 6.5, and 9 mm), and relative density (10–30%). They have proved the manufacturability of SLM for porous structures. The main conclusions come out that the relative density has a dominant

effect on heat storage performances, subsequently followed by cell architecture and cell. Further, research on the optimal design of the TPMS-PCMs is expected in future work.

The high thermal conductivity of metal foam can increase the effective thermal conductivity and the overall heat transfer rate. However, the existence of metal foam inhibits the liquid salt motion, resulting in a minimised natural convection effect. Therefore, the metal foam pore density and distributions can be significant parameters to be optimised.

4.2.3. Additive manufactured form-stable composite PCMs

Composite PCMs can be able to overcome the molten salt level challenges. The PCM devices have attracted attention in different fields including energy harvesting devices, buildings, and wearable devices [166,167]. Nofal *et al*. [168,169] developed an expanded graphite/paraffin wax phase change composite, as illustrated in Figure 13 (a). The paraffin wax is initially melted and then impregnated into the inter-particle pores of expanded graphite through capillaries. These two materials were built at a micro-scale (50–200 microns) by a layer-by-layer SLS technique. Samples with diverse layers were fabricated and tested. Experimental results demonstrated the thermal conductivity in a range of 0.83–0.92 W m^{-1} K^{-1}, and the latent heat in a range of 150–156 kJ·kg^{-1}, showing the effectiveness of
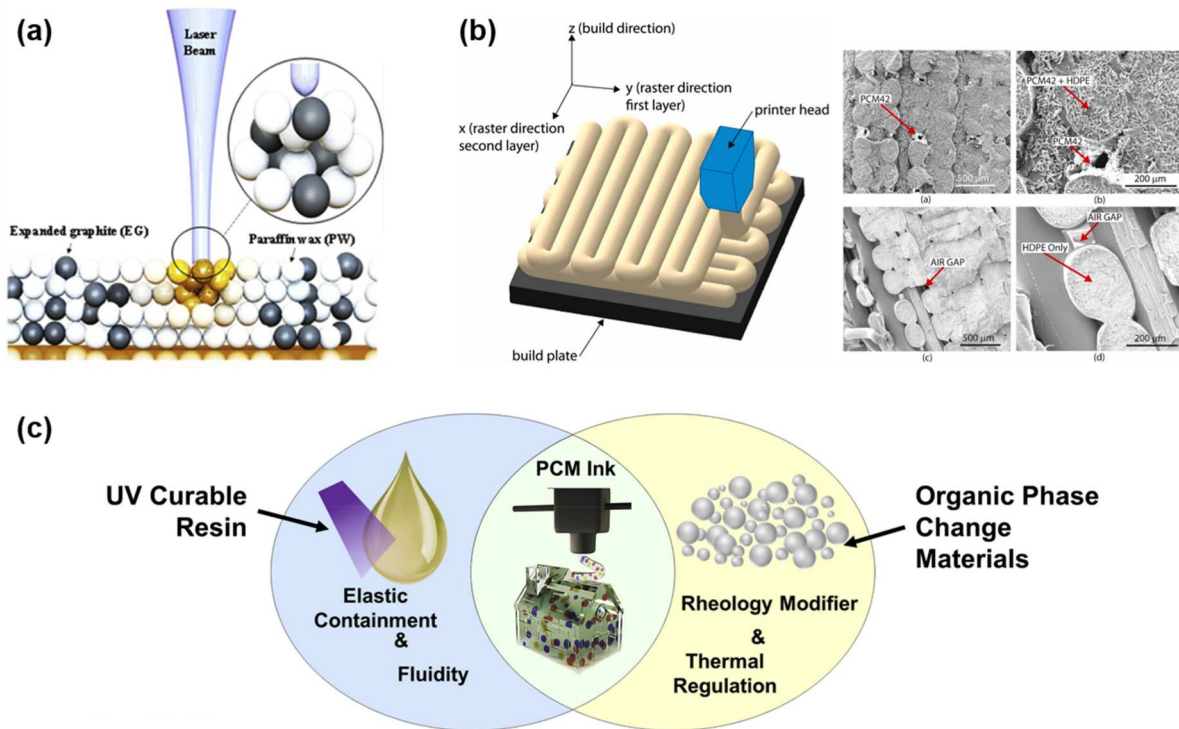
Figure 13. Demonstration of additive manufacturing of composite PCMs: (a) SLS process of paraffin wax/expanded graphite [168] (b) FFF process of composite PCMs, and illustration of printed samples e.g. PCM42/HDPE and HDPE [171] (c) DIW process of the polymer-PCM composites [173].

the nonconventional manufacturing technique for fabricating PCMs. The 3D printed composite PCMs were further used for the thermal management of lithium-ion battery cells [169].

Rigotti *et al*. [170] fabricated an innovative thermoplastic polyurethan (TPU) blend with encapsulated PCM using FDM technology. An effective energy storage and release capability was acquired in the 3D printed samples with a melting enthalpy value of 70 J/g. In addition, the hard shells of the microcapsules have an improvement of stiffness and a reduction of the elongation at break. Freeman *et al*. [171] encapsulated PCM into polymer filament using FFF technology (Figure 13 (b)). A composite containing 40% PureTemp 42 by mass was mixed with high-density polyethylene (HDPE) and extruded to make filaments. Experimental results show that the TES capability of the composite filament effectively acts as if there is 31.8% of the pure PCM42. The phase change temperature of the composite filament decreases compared with pure PCM42 or HDPE. Nonetheless, the thermal conductivities of the printed composites were decreased compared with the molded composite, due to air gaps formed during the printing process. Recently, Singh et al. fabricated PCM devices using FDM 3D printing [172]. A composite nylon-based filament with 69.0 ± 0.50 J/g latent heat was developed. This research demonstrates the

integration of composite PCMs with complex geometrical designs.

DIW is one of the most used 3D printing techniques for energy storage materials. Wei et al. [173] proposed a facile method to print PCM-filled inks by DIW techniques. As shown in Figure 13(c), organic PCMs were used to optimise viscosities and thermal energy storage properties. The PCM beads were dispersed in acrylate resin and cured with UV light. By using the developed inks, the 3D printed house can maintain a 40% lower temperature compared with the houses without PCM. Recently, phase change based electronic packaging materials were developed by Feng et al. [174]. The composite PCMs developed in this work contain 70% paraffin and a latent heat of 145.6 J/g. By adjusting the printing parameters, complex 2D and 3D patterns can be fabricated according to the circuits structure.

3D printing offers a flexible way to integrate composite PCMs into functional devices. One unique application is phase change fabrics for wearable devices. Ma et al. [166] developed a series of 3D printable phase change polysiloxane networks with a temperature range from 24.9 and 53.6 °C, and latent heat from 24.9 J/g to 125.3 J/g. By combining carbon fibre cloth, a phase change composite was fabricated for wearable devices. Yang et al. [175] developed phase change nonwoven fabrics by using single-walled carbon nanotubes

(SWNT). The 3D printed flexible sheets with 1 wt.% SWNT have a 0.52 Wm^{-1}K^{-1} thermal conductivity and 65 J g^{-1} latent heat.

5. Future perspectives

Additive manufacturing offers a new way to fabricate the next-generation energy storage devices. However, numerical modelling, material development, and performance evaluation for AM processes in the energy storage field are insufficient. Figure 14 illustrates a multiscale digital and physical research roadmap for AM energy storage techniques. Relevant fundamental research using advanced numerical tools is scarce, especially an integrated framework considering digital design and manufacturing process needs to be developed. Future perspectives considering both digital design and physical AM processes are presented in the following.

5.1. Digital design

Digital design approach opens up the opportunity to automatically tailor the optimal parameters and configurations with the best performance. Process modelling such as particle scale simulations can help to optimise AM processes and select appropriate parameters. With a multi-physics numerical modelling approach, the inherent transport mechanisms of energy storage devices can be clearly understood. An integrated numerical framework of process-microstructure-performance will contribute to significantly reducing the timescale of energy storage device design and manufacturing.

(a) Process modelling. Numerical modelling is useful to understand the inherent physical mechanisms and material interactions during AM. Process modelling on multiple lengths and time scales is a powerful tool to understand how the manufacturing parameters affect the final product quality. Powder bed based AM has been widely studied using numerical models such as discrete element method (DEM), lattice Boltzmann (LB), and finite element analysis [177]. Manufacturing issues such as powder spreading, layer bonding defects, and melt pool dynamics have been studied [177,178]. The active powder materials used in energy storage devices have some unique physical properties such as adhesive forces, and particle shapes that need to be properly considered in numerical modelling. As most electrochemical energy storage devices are fabricated via the DIW technique, multi-physics numerical models in this field are necessary. The adhesion forces between layers, and
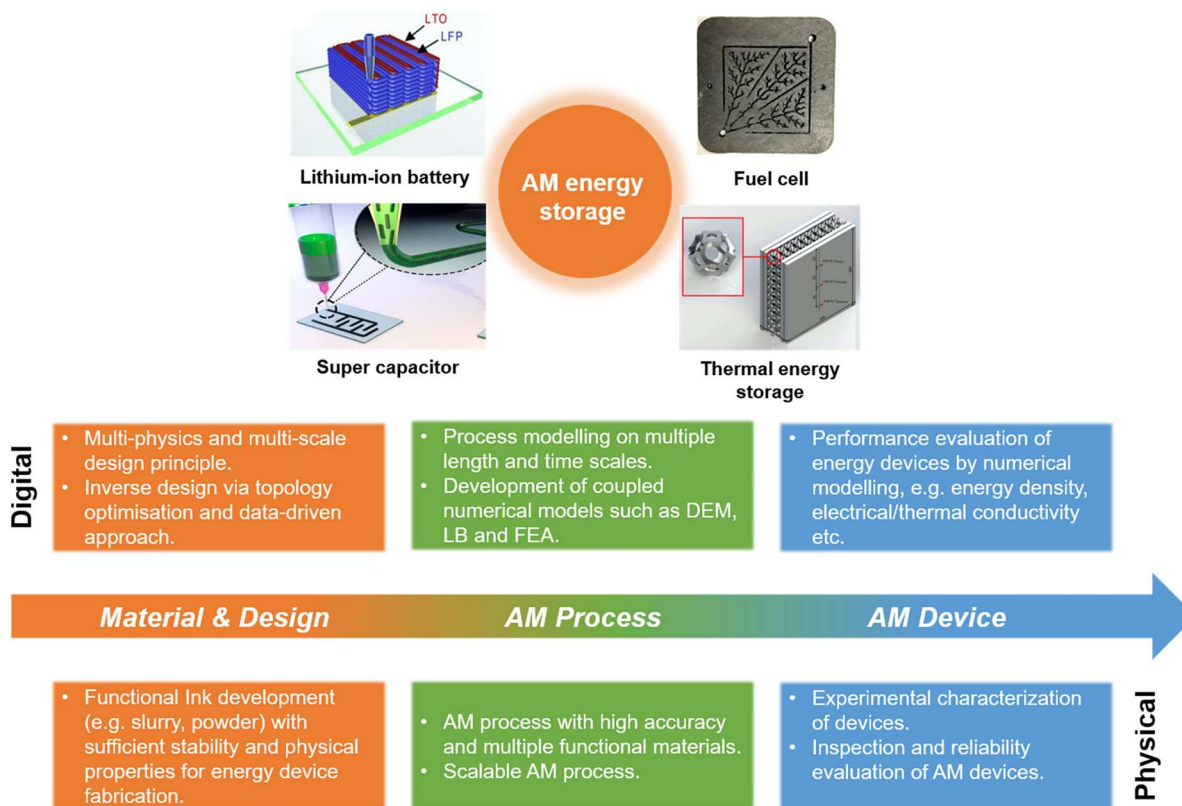
Figure 14. Multiscale digital and physical research roadmap for AM energy storage techniques [27,74,129,135].

the deposition of molten materials on the substrate need to be clearly understood considering different ink properties and process parameters [179].

(b) Design principle. The combination of digital design and additive manufacturing offers a new way for next-generation energy storage techniques. For the energy storage technique, the design principle needs to consider the integration of material property, microstructure, and performance across multiple temporal and spatial scales [180]. Some design strategies were discussed in Section 2. The conventional device design is usually very time-consuming and through trial-and-error. For an energy storage device, the energy density and charge/discharge rate usually contradict each other. Take the lithium-ion battery as an example, energy density can be increased by thick electrodes, however, the rate performance usually decreases due to increased diffusion distances in thick electrodes. Therefore, advanced simulation methods considering multi-physical properties (mechanical, thermal, and electrical) need to be developed to guide the design of functional energy devices. The combination of multi-physics numerical modelling and data-driven design offers a powerful way for the next generation energy storage device design [180].

(c) Digital design and optimization strategies at the micro/nanoscale. Digital design and optimisation strategies have been used to design materials in a micro/nano scale. Zheng et al. fabricated octet micro lattices that showed exceptionally stiff, strong properties. The resulting hollow tube of micro lattices has a minimum thickness from ∼40 to 210 nm [10]. Topology optimisation is commonly used to maximise the device performance. The multiscale topology optimisation approach has the advantage to optimise structural features at different scales [181]. Chen et al. [182] proposed a nano-topology optimisation approach that can design materials atom by atom. As hierarchical features at different scales commonly exist in energy storage devices, in future these complex 3D microscale/nanoscale structures need to be fabricated by using state of art micro AM techniques, e.g. projection micro-stereo lithography [183].

5.2. Additive manufacturing process

By using AM techniques, the functional devices with controlled compositions are manufactured in a facile way by avoiding the post-steps of assembly and packaging. In the energy storage field, AM paves the way to fabricate devices with quick charge/discharge performance. The ink development and printing resolution are keys to advance energy storage manufacturing. In addition, cost-effective mass manufacturability is necessary in application to industry.

(a) Ink development. In this work, AM techniques with different physical processes are reviewed, as listed in Table 2. A proper selection of AM techniques according to the functions, printing accuracy, and material properties is needed. Take the electrochemical energy storage device as an example, DIW is a mainstream technique. However, most inks are in-house made with desired electrical properties and viscosities. More efforts are still needed to develop inks containing active materials such as carbon, metallic oxide, and PCMs with sufficient stability and viscosity. Materials in solid forms such as micro-sized powders and filaments are commonly used for powder bed fusion and material extrusion AM processes. Therefore, the development of commercially accessible active material inks in solid forms is meaningful to widen applications of AM in the energy storage field.

(b) Printing resolution & Anisotropy. Currently, most AM systems can only produce features larger than a millimetre. Hierarchical structures containing multiple length scale pores are commonly used in energy devices. Traditionally, self-assembling and template approaches are used to tailor the pore size at the nanoscale. The micro and the nano-scale structures can only be achieved using specific AM techniques [22,184]. The development of multi-scale and multi-material AM is important to fabricate functional energy materials with hierarchical microstructures. By using the photopolymerization process, hierarchical metamaterials with nanoscale features have been fabricated [10].

As additive manufacturing constructs 3D objects in a layer-wise manner, this results in anisotropic performances along different directions. These anisotropic behaviours are usually undesired. However, manipulating anisotropic structures via additive manufacturing to achieve desired functionalities has widespread emerging applications in aerospace and tissue engineering industries [185]. It is worth further investigating the effect of anisotropic materials on the energy storage device performance.

(c) Scale up. The manufacturing cost of AM techniques for large-scale applications is also a big issue. Most AM processes are still on a laboratory scale, used for prototypes and concepts. Development of high-speed, scalable AM processes is necessary. Economic analysis shows that the application of 3D printing for energy storage fabrication is still not a simple and economical strategy. For the thermal energy storage device, recent work has shown that the unit price ratio between the additive manufactured thermal enhancement technique and PCMs should be less than 6 as an economical solution [160].

6. Conclusion

This review outlines the current application of AM techniques in the energy storage field. Firstly, the digital design approach and mainstream AM techniques are discussed. Recent applications of AM techniques in the energy storage field such as lithium-ion battery, fuel cell, supercapacitor, and thermal energy storage systems are summarised. In the end, a discussion of future perspectives is given.

The optimised design of structured components can improve energy conversion and storage efficiency. The main digital design and optimisation strategies are discussed in this review, including lattice structures, naturally occurring structures, topology optimisation and data-driven design. The AM technique offers a promising way to fabricate the optimised designs with unique properties. For energy storage applications, a proper selection of AM techniques according to the printing resolution and materials is necessary.

From future perspectives there are still some technical challenges that need to be tackled:

(1) Rationale design approach development. Complex multiphysics exists in energy storage systems. The device performance is highly dependent on material compositions, microstructure design, and manufacturing parameters. A digital workflow with sophisticated numerical models needs to be developed to optimise physical AM processes and microstructure design.
(2) Ink material development. Commercially available ink materials used for high-resolution AM techniques need to be further investigated. Take lithium-ion batteries as an example, DIW is mainly used to fabricate multiple-layer energy storage devices. New ink formulations with improved properties need to be further developed that can be applied to the material extrusion process.
(3) New AM process development. There are various AM techniques as listed in Table 2. In most cases, a certain printing process can only be used for specific purposes. For the commercial viability of AM energy storage systems, one key issue is economic efficiency. New AM processes with a wider application scope and mass manufacturability are expected to be developed.

Acknowledgement

Disclosure statement

Funding

Data availability

Data will be made available on request.

References

[1] Iyer G, Ou Y, Edmonds J, et al. Ratcheting of climate pledges needed to limit peak global warming. Nat Clim Change. 2022;12(12):1129–1135.
[2] The United Nations. For a livable climate: Net-zero commitments must be backed by credible action. Available from: https://www.un.org/en/climatechange/net-zero-coalition.
[3] Cárdenas B, Swinfen-Styles L, Rouse J, et al. Energy storage capacity vs. renewable penetration: a study for the UK. Renewable Energy. 2021;171:849–867.
[4] Koohi-Fayegh S, Rosen MA. A review of energy storage types, applications and recent developments. J Energy Storage. 2020;27:101047.
[5] Ge R, Cumming DJ, Smith RM. Discrete element method (DEM) analysis of lithium ion battery electrode structures from X-ray tomography-the effect of calendering conditions. Powder Technol. 2022;403:117366.
[6] Li Q, Wei W, Li Y, et al. Development and investigation of form-stable quaternary nitrate salt based composite phase change material with extremely low melting temperature and large temperature range for low-mid thermal energy storage. Energy Rep. 2022;8:1528–1537.
[7] Grant PS, Greenwood D, Pardikar K, et al. Roadmap on Li-ion battery manufacturing research. J Phys: Energy. 2022;4(4):042006.
[8] Ge R, Ghadiri M, Bonakdar T, et al. Deformation of 3D printed agglomerates: multiscale experimental tests and DEM simulation. Chem Eng Sci. 2020;217:115526.
[9] Ge R, Ghadiri M, Bonakdar T, et al. 3D printed agglomerates for granule breakage tests. Powder Technol. 2017;306:103–112.
[10] Zheng X, Lee H, Weisgraber TH, et al. Ultralight, ultrastiff mechanical metamaterials. Science. 2014;344(6190):1373–1377.
[11] Pham M-S, Liu C, Todd I, et al. Damage-tolerant architected materials inspired by crystal microstructure. Nature. 2019;565(7739):305–311.
[12] Ge R, Humbert G, Martinez R, et al. Additive manufacturing of a topology-optimised multi-tube energy storage device: experimental tests and numerical analysis. Appl Therm Eng. 2020;180:115878.
[13] Rasaki S, Liu C, Lao C, et al. The innovative contribution of additive manufacturing towards revolutionizing fuel cell fabrication for clean energy generation: a

comprehensive review. Renewable Sustainable Energy Rev. 2021;148:111369.

[14] Jafari D, Wits WW. The utilization of selective laser melting technology on heat transfer devices for thermal energy conversion applications: a review. Renewable Sustainable Energy Rev. 2018;91:420–442.

[15] Pang Y, Cao Y, Chu Y, et al. Additive manufacturing of batteries. Adv Funct Mater. 2020;30(1):1906244.

[16] Pizzolato A, Sharma A, Ge R, et al. Maximization of performance in multi-tube latent heat storage–optimization of fins topology, effect of materials selection and flow arrangements. Energy. 2020;203:114797.

[17] Freeman TB, Foster KE, Troxler CJ, et al. Advanced materials and additive manufacturing for phase change thermal energy storage and management: a review. Adv Energy Mater. 2023;13:2204208.

[18] Tian X, Jin J, Yuan S, et al. Emerging 3D-printed electrochemical energy storage devices: a critical review. Adv Energy Mater. 2017;7(17):1700127.

[19] Zhang H, Yu X, Braun PV. Three-dimensional bicontinuous ultrafast-charge and-discharge bulk battery electrodes. Nat Nanotechnol. 2011;6(5):277–281.

[20] Zhu C, Han T, Duoss EB, et al. Highly compressible 3D periodic graphene aerogel microlattices. Nat Commun. 2015;6(1):1–8.

[21] Trembacki BL, Vadakkepatt A, Roberts SA, et al. Volume-averaged electrochemical performance modeling of 3D interpenetrating battery electrode architectures. J Electrochem Soc. 2019;167(1):013507.

[22] Choudhury S, Agrawal M, Formanek P, et al. Nanoporous cathodes for high-energy Li–S batteries from gyroid block copolymer templates. ACS Nano. 2015;9(6):6147–6157.

[23] Werner J, Rodríguez-Calero G, Abruña H, et al. Block copolymer derived 3-D interpenetrating multifunctional gyroidal nanohybrids for electrical energy storage. Energy Environ Sci. 2018;11(5):1261–1270.

[24] Mitchell SL, Ortiz M. Computational multiobjective topology optimization of silicon anode structures for lithium-ion batteries. J Power Sources. 2016;326:242–251.

[25] Deva A, Krs V, Robinson LD, et al. Data driven analytics of porous battery microstructures. Energy Environ Sci. 2021;14(4):2485–2493.

[26] Zhang Y, Ma G, Wang J, et al. Numerical and experimental study of phase-change temperature controller containing graded cellular material fabricated by additive manufacturing. Appl Therm Eng. 2019;150:1297–1305.

[27] Diani A, Nonino C, Rossetto L. Melting of phase change materials inside periodic cellular structures fabricated by additive manufacturing: experimental results and numerical simulations. Appl Therm Eng. 2022;215:118969.

[28] Hu X, Gong X. Experimental and numerical investigation on thermal performance enhancement of phase change material embedding porous metal structure with cubic cell. Appl Therm Eng. 2020;175:115337.

[29] Qureshi ZA, Al-Omari SAB, Elnajjar E, et al. Using triply periodic minimal surfaces (TPMS)-based metal foams structures as skeleton for metal-foam-PCM composites for thermal energy storage and energy management applications. Int Commun Heat Mass Transfer. 2021;124:105265.

[30] Ramazani H, Kami A. Metal FDM, a new extrusion-based additive manufacturing technology for manufacturing of metallic parts: a review. Prog Addit Manuf. 2022;7:1–18.

[31] Tavakoli A, Hashemi J, Najafian M, et al. Physics-based modelling and data-driven optimisation of a latent heat thermal energy storage system with corrugated fins. Renewable Energy. 2023:119200.

[32] Torquato S, Hyun S, Donev A. Multifunctional composites: optimizing microstructures for simultaneous transport of heat and electricity. Phys Rev Lett. 2002;89 (26):266601.

[33] Wegst UG, Bai H, Saiz E, et al. Bioinspired structural materials. Nat Mater. 2015;14(1):23–36.

[34] Van Dijk NP, Maute K, Langelaar M, et al. Level-set methods for structural topology optimization: a review. Struct Multidiscipl Optim. 2013;48(3):437–472.

[35] Pizzolato A. Topology optimization for energy problems. Torino: Politecnico di Torino; 2018.

[36] Panesar A, Abdi M, Hickman D, et al. Strategies for functionally graded lattice structures derived using topology optimisation for additive manufacturing. Addit Manuf. 2018;19:81–94.

[37] Miskin MZ, Khaira G, de Pablo JJ, et al. Turning statistical physics models into materials design engines. Proc Natl Acad Sci USA. 2016;113(1):34–39.

[38] Xue D, Balachandran PV, Hogden J, et al. Accelerated search for materials with targeted properties by adaptive design. Nat Commun. 2016;7(1):1–9.

[39] Bastek J-H, Kumar S, Telgen B, et al. Inverting the structure–property map of truss metamaterials by deep learning. Proc Natl Acad Sci USA. 2022;119(1):e2111505119.

[40] Moghadam PZ, Rogge SM, Li A, et al. Structure-mechanical stability relations of metal-organic frameworks via machine learning. Matter. 2019;1(1):219–234.

[41] Human bone. Available from: https://statnano.com/news/68390/Batteries-Mimic-Mammal-Bones-for-Stability.

[42] Bubbles. Available from: https://www.pinterest.co.uk/pin/315463148889921735/.

[43] Honeycomb. Available from: https://www.pinterest.co.uk/pin/370913719314630083/.

[44] Nathan Myhrvold, Travel & photo essays: Snow flakes. Available from: http://nathanmyhrvold.com/index.php/travel/essay/snowflakes.

[45] Pham M, Ahn H. Experimental optimization of a hybrid foil–magnetic bearing to support a flexible rotor, experimental optimization of a hybrid foil-magnetic bearing to support a flexible rotor. Mech Syst Signal Process. 2014;46. Available from: https://www.pinterest.co.uk/pin/369998925645095791/.

[46] Cong F, Chen J, Dong G, et al. Experimental validation of impact energy model for the rub–impact assessment in a roto rsystem. Mech Syst Signal Process. 2011;25. Available from: https://www.pinterest.co.uk/pin/72409506501318858/.

[47] Fan C, Pan M. Fluid-induced instability elimination of rotor-bearing system with an electromagnetic exciter. Int J Mech Sci. 2010;52(4). Available from: https://www.featool.com/model_showcase/03_structural_mechanics_07_topology_optimization1/.

[48] Jung Y, Torquato S. Fluid permeabilities of triply periodic minimal surfaces. Phys Rev E. 2005;72(5):056319.

[49] Mirzendehdel AM, Rankouhi B, Suresh K. Strength-based topology optimization for anisotropic parts. Addit Manuf. 2018;19:104–113.

[50] Langelaar M. Topology optimization of 3D self-supporting structures for additive manufacturing. Addit Manuf. 2016;12:60–70.

[51] Zhakeyev A, Wang P, Zhang L, et al. Additive manufacturing: unlocking the evolution of energy materials. Adv Sci. 2017;4(10):1700187.

[52] Gulzar U, Glynn C, O'Dwyer C. Additive manufacturing for energy storage: methods, designs and material selection for customizable 3D printed batteries and supercapacitors. Curr Opin Electrochem. 2020;20:46–53.

[53] Ian Gibson IG. *Additive manufacturing technologies 3D printing, rapid prototyping, and direct digital manufacturing*. New York: Springer; 2015.

[54] Sun C, Wang Y, McMurtrey MD, et al. Additive manufacturing for energy: a review. Appl Energy. 2021;282:116041.

[55] Huang Z, Shao G, Li L. Micro/nano functional devices fabricated by additive manufacturing. Prog Mater Sci. 2022;131:101020.

[56] Hoath SD, Harlen OG, Hutchings IM. Jetting behavior of polymer solutions in drop-on-demand inkjet printing. J Rheol. 2012;56(5):1109–1127.

[57] Oh Y, Bharambe V, Mummareddy B, et al. Cortes, Microwave dielectric properties of zirconia fabricated using NanoParticle Jetting™, Additive Manufacturing. 2019:27;586–594.

[58] Unkovskiy S, Spintzyk J, Brom F, et al. Direct 3D printing of silicone facial prostheses: A preliminary experience in digital workflow. J Prosthet Dent 2014;120(2):303–308.

[59] Hou Y, Gao M, Chen J, et al. Preparation of iron oxide–coated aramid fibres for improving the mechanical performance and flame retardancy of multi jet fusion–printed polyamide 12 composites. Virtual Phys Prototyp. 2023;18(1):e2171892.

[60] Desktop metal, What is single pass jetting. Available from: https://www.desktopmetal.com/resources/what-is-single-pass-jetting.

[61] Bae C-J, Diggs AB, Ramachandran A. Quantification and certification of additive manufacturing materials and processes, Additive manufacturing. Elsevie(r2018):181–213.

[62] 3DEXPERIENCE, 3D priting - addtive: Directed energy deposition - DED, LENS, EBAM. Available from: https://make.3dexperience.3ds.com/processes/directed-energy-deposition.

[63] Gibson I, Rosen D, Stucker B. *Vat photopolymerization processes, additive manufacturing technologies*. New York: Springer; 2015. pp. 63–106.

[64] King WE, Anderson AT, Ferencz RM, et al. Laser powder bed fusion additive manufacturing of metals; physics, computational, and materials challenges. Appl Phys Rev. 2015;2(4):041304.

[65] Kristiawan RB, Imaduddin F, Ariawan D, et al. A review on the fused deposition modeling (FDM) 3D printing: filament processing,: materials, and printing parameters. Open Eng. 2021;11(1):639–649.

[66] Mora S, Pugno NM, Misseroni D. 3D printed architected lattice structures by material jetting. Mater Today. 2022;59:107–132.

[67] Ziaee M, Crane NB. Binder jetting: a review of process, materials, and methods. Addit Manuf. 2019;28:781–801.

[68] Dass A, Moridi A. State of the art in directed energy deposition: from additive manufacturing to materials design. Coatings. 2019;9(7):418.

[69] Svetlizky D, Das M, Zheng B, et al. Directed energy deposition (DED) additive manufacturing: physical characteristics, defects, challenges and applications. Mater Today. 2021;49:271–295.

[70] Tan HW, Choong YYC, Kuo CN, et al. 3D printed electronics: processes, materials and future trends. Prog Mater Sci. 2022;127:100945.

[71] Moon H, Miljkovic N, King WP. High power density thermal energy storage using additively manufactured heat exchangers and phase change material. Int J Heat Mass Tran. 2020;153:119591.

[72] Woods J, Mahvi A, Goyal A, et al. Rate capability and Ragone plots for phase change thermal energy storage. Nat Energy. 2021;6(3):295–302.

[73] Tian X, Zhou K. 3D printing of cellular materials for advanced electrochemical energy storage and conversion. Nanoscale. 2020;12(14):7416–7432.

[74] Sun K, Wei TS, Ahn BY, et al. 3D printing of interdigitated Li-Ion microbattery architectures. Adv Mater. 2013;25 (33):4539–4543.

[75] Ning H, Pikul JH, Zhang R, et al. Holographic patterning of high-performance on-chip 3D lithium-ion microbatteries. Proc Natl Acad Sci USA. 2015;112(21):6573–6578.

[76] Ho CC, Murata K, Steingart DA, et al. A super ink jet printed zinc–silver 3D microbattery. J Micromech Microeng. 2009;19(9):094013.

[77] Fu K, Wang Y, Yan C, et al. Graphene oxide-based electrode inks for 3D-printed lithium-ion batteries. Adv Mater. 2016;28(13):2587–2594.

[78] Shen K, Mei H, Li B, et al. 3D printing sulfur copolymer-graphene architectures for Li-S batteries. Adv Energy Mater. 2018;8(4):1701527.

[79] Lacey SD, Kirsch DJ, Li Y, et al. Extrusion-based 3D printing of hierarchically porous advanced battery electrodes. Adv Mater. 2018;30(12):1705651.

[80] Maurel A, Courty M, Fleutot B, et al. Highly loaded graphite–polylactic acid composite-based filaments for lithium-ion battery three-dimensional printing. Chem Mater. 2018;30(21):7484–7493.

[81] Narita K, Citrin MA, Yang H, et al. 3D architected carbon electrodes for energy storage. Adv Energy Mater. 2021;11(5):2002637.

[82] Yee DW, Citrin MA, Taylor ZW, et al. Hydrogel-Based additive manufacturing of lithium cobalt oxide. Adv Mater Technol. 2021;6(2):2000791.

[83] Saleh MS, Li J, Park J, et al. 3D printed hierarchically-porous microlattice electrode materials for exceptionally high specific capacity and areal capacity lithium ion batteries. Addit Manuf. 2018;23:70–78.

[84] Deiner LJ, Jenkins T, Powell A, et al. High capacity rate capable aerosol Jet printed Li-Ion battery cathode. Adv Eng Mater. 2019;21(5):1801281.

[85] Deiner LJ, Jenkins T, Howell T, et al. Aerosol Jet printed polymer composite electrolytes for solid-state Li-Ion batteries. Adv Eng Mater. 2019;21(12):1900952.

[86] Hu J, Jiang Y, Cui S, et al. 3D-printed cathodes of LiMn1−xFexPO4 nanocrystals achieve both ultrahigh rate and high capacity for advanced lithium-ion battery. Adv Energy Mater. 2016;6(18):1600856.

[87] Wang Z, Ni J, Li L, et al. Theoretical simulation and modeling of three-dimensional batteries. Cell Rep Phys Sci. 2020;1(6):100078.

[88] Ragones H, Vinegrad A, Ardel G, et al. On the road to a multi-coaxial-cable battery: development of a novel 3D-printed composite solid electrolyte. J Electrochem Soc. 2019;167(7):070503.

[89] Wang J, Sun Q, Gao X, et al. Toward high areal energy and power density electrode for Li-ion batteries via optimized 3D printing approach. ACS Appl Mater Interfaces. 2018;10(46):39794–39801.

[90] Han J, Johnson I, Chen M. 3D continuously porous graphene for energy applications. Adv Mater. 2021;34:2108750.

[91] Zekoll S, Marriner-Edwards C, Hekselman AO, et al. Hybrid electrolytes with 3D bicontinuous ordered ceramic and polymer microchannels for all-solid-state batteries. Energy Environ Sci. 2018;11(1):185–201.

[92] Wang Y, Chen C, Xie H, et al. 3D-printed all-fiber li-ion battery toward wearable energy storage. Adv Funct Mater. 2017;27(43):1703140.

[93] Reyes C, Somogyi R, Niu S, et al. Three-dimensional printing of a complete lithium ion battery with fused filament fabrication. ACS Appl Energy Mater. 2018;1 (10):5268–5279.

[94] Acord KA, Dupuy AD, Bertoli US, et al. Morphology, microstructure, and phase states in selective laser sintered lithium ion battery cathodes. J Mater Process Technol. 2021;288:116827.

[95] Cohen E, Menkin S, Lifshits M, et al. Novel rechargeable 3D-microbatteries on 3D-printed-polymer substrates: feasibility study. Electrochim Acta. 2018;265:690–701.

[96] Saccone MA, Greer JR. Understanding and mitigating mechanical degradation in lithium–sulfur batteries: additive manufacturing of Li2S composites and nano-mechanical particle compressions. J Mater Res. 2021;36 (18):3656–3666.

[97] Chen Q, Xu R, He Z, et al. Printing 3D gel polymer electrolyte in lithium-ion microbattery using stereolithography. J Electrochem Soc. 2017;164(9):A1852.

[98] Li J, Liang X, Liou F, et al. Macro-/micro-controlled 3D lithium-ion batteries via additive manufacturing and electric field processing. Sci Rep. 2018;8(1):1–11.

[99] Liu C, Xu F, Cheng X, et al. Comparative study on the electrochemical performance of LiFePO4 cathodes fabricated by low temperature 3D printing, direct ink writing and conventional roller coating process. Ceram Int. 2019;45(11):14188–14197.

[100] Gao X, Sun Q, Yang X, et al. Toward a remarkable Li-S battery via 3D printing. Nano Energy. 2019;56:595–603.

[101] Chen C, Jiang J, He W, et al. 3D printed high-loading lithium-sulfur battery toward wearable energy storage. Adv Funct Mater. 2020;30(10):1909469.

[102] Wei TS, Ahn BY, Grotto J, et al. 3D printing of customized Li-ion batteries with thick electrodes. Adv Mater. 2018;30(16):1703027.

[103] Shen K, Cao Z, Shi Y, et al. 3D printing lithium salt towards dendrite-free lithium anodes. Energy Storage Mater. 2021;35:108–113.

[104] Moser S, Kenel C, Wehner LA, et al. 3D ink-printed, sintered porous silicon scaffolds for battery applications. J Power Sources. 2021;507:230298.

[105] Cao D, Xing Y, Tantratian K, et al. 3D printed high-performance lithium metal microbatteries enabled by nanocellulose. Adv Mater. 2019;31(14):1807313.

[106] Qiao Y, Liu Y, Chen C, et al. 3D-printed graphene oxide framework with thermal shock synthesized nanoparticles for Li-CO2 batteries. Adv Funct Mater. 2018;28 (51):1805899.

[107] McOwen DW, Xu S, Gong Y, et al. 3D-printing electrolytes for solid-state batteries. Adv Mater. 2018;30 (18):1707132.

[108] Blake AJ, Kohlmeyer RR, Hardin JO, et al. 3D printable ceramic–polymer electrolytes for flexible high-performance li-ion batteries with enhanced thermal stability. Adv Energy Mater. 2017;7(14):1602920.

[109] Cheng M, Jiang Y, Yao W, et al. Elevated-temperature 3D printing of hybrid solid-state electrolyte for Li-ion batteries. Adv Mater. 2018;30(39):1800615.

[110] Zhou L, Ning W, Wu C, et al. 3D-printed microelectrodes with a developed conductive network and hierarchical pores toward high areal capacity for microbatteries. Adv Mater Technol. 2019;4(2):1800402.

[111] Lyu Z, Lim GJ, Guo R, et al. 3D-printed MOF-derived hierarchically porous frameworks for practical high-energy density Li–O2 batteries. Adv Funct Mater. 2019;29 (1):1806658.

[112] Thakur A, Dong X. Additive manufacturing of 3D structural battery composites with coextrusion deposition of continuous carbon fibers. Manuf Lett. 2020;26:42–47.

[113] Ragones H, Menkin S, Kamir Y, et al. Towards smart free form-factor 3D printable batteries. Sustainable Energy Fuels. 2018;2(7):1542–1549.

[114] Maurel A, Grugeon S, Fleutot B, et al. Three-dimensional printing of a LiFePO4/graphite battery cell via fused deposition modeling. Sci Rep. 2019;9(1):1–14.

[115] Valera-Jiménez JF, Pérez-Flores JC, Castro-García M, et al. Development of full ceramic electrodes for lithium-ion batteries via desktop-fused filament fabrication and further sintering. Appl Mater Today. 2021;25:101243.

[116] Delannoy P-E, Riou B, Brousse T, et al. Ink-jet printed porous composite LiFePO4 electrode from aqueous suspension for microbatteries. J Power Sources. 2015;287:261–268.

[117] Young D, Sukeshini A, Cummins R, et al. Ink-jet printing of electrolyte and anode functional layer for solid oxide fuel cells. J Power Sources. 2008;184(1):191–196.

[118] Li C, Shi H, Ran R, et al. Thermal inkjet printing of thin-film electrolytes and buffering layers for solid oxide fuel cells with improved performance. Int J Hydrogen Energy. 2013;38(22):9310–9319.

[119] Pham TT, Tu HP, Dao TD, et al. Fabrication of an anode functional layer for an electrolyte-supported solid oxide fuel cell using electrohydrodynamic jet printing. Adv Nat Sci: Nanosci Nanotechnol. 2019;10 (1):015004.

[120] Yu C-C, Baek JD, Su C-H, et al. Inkjet-printed porous silver thin film as a cathode for a low-temperature solid oxide fuel cell. ACS Appl Mater Interfaces. 2016;8(16):10343–10349.

[121] Mitchell-Williams TB, Tomov RI, Saadabadi S, et al. Infiltration of commercially available, anode supported SOFC's via inkjet printing. Materials for Renewable and Sustainable Energy. 2017;6(2):1–9.

[122] Wang C, Tomov R, Mitchell-Williams T, et al. Inkjet printing infiltration of Ni-Gd: CeO2 anodes for low temperature solid oxide fuel cells. J Appl Electrochem. 2017;47(11):1227–1238.

[123] Masciandaro S, Torrell M, Leone P, et al. Three-dimensional printed yttria-stabilized zirconia self-supported electrolytes for solid oxide fuel cell applications. J Eur Ceram Soc. 2019;39(1):9–16.

[124] Pesce A, Hornés A, Núñez M, et al. 3D printing the next generation of enhanced solid oxide fuel and electrolysis cells. J Mater Chem A. 2020;8(33):16926–16932.

[125] Guo N, Leu MC. Effect of different graphite materials on the electrical conductivity and flexural strength of bipolar plates fabricated using selective laser sintering. Int J Hydrogen Energy. 2012;37(4):3558–3566.

[126] Gould BD, Rodgers JA, Schuette M, et al. Performance and limitations of 3D-printed bipolar plates in fuel cells. ECS J Solid State Sci Technol. 2015;4(4):P3063.

[127] Ramos-Alvarado B, Hernandez-Guerrero A, Elizalde-Blancas F, et al. Constructal flow distributor as a bipolar plate for proton exchange membrane fuel cells. Int J Hydrogen Energy. 2011;36(20):12965–12976.

[128] Fan Z, Zhou X, Luo L, et al. Experimental investigation of the flow distribution of a 2-dimensional constructal distributor. Exp Therm Fluid Sci. 2008;33(1):77–83.

[129] Guo N, Leu MC, Koylu UO. Bio-inspired flow field designs for polymer electrolyte membrane fuel cells. Int J Hydrogen Energy. 2014;39(36):21185–21195.

[130] Xing B, Cao C, Zhao W, et al. Dense 8 mol% yttria-stabilized zirconia electrolyte by DLP stereolithography. J Eur Ceram Soc. 2020;40(4):1418–1423.

[131] Bian B, Wang C, Hu M, et al. Application of 3D printed porous copper anode in microbial fuel cells. Front Energy Res. 2018;6:50.

[132] Xing B, Yao Y, Meng X, et al. Self-supported yttria-stabilized zirconia ripple-shaped electrolyte for solid oxide fuel cells application by digital light processing three-dimension printing. Scr Mater. 2020;181:62–65.

[133] Taylor AD, Kim EY, Humes VP, et al. Inkjet printing of carbon supported platinum 3-D catalyst layers for use in fuel cells. J Power Sources. 2007;171(1):101–106.

[134] Beidaghi M, Gogotsi Y. Capacitive energy storage in micro-scale devices: recent advances in design and fabrication of micro-supercapacitors. Energy Environ Sci. 2014;7(3):867–884.

[135] Orangi J, Hamade F, Davis VA, et al. 3D printing of additive-free 2D Ti3C2T x (MXene) ink for fabrication of micro-supercapacitors with ultra-high energy densities. ACS Nano. 2019;14(1):640–650.

[136] Azhari A, Marzbanrad E, Yilman D, et al. Binder-jet powder-bed additive manufacturing (3D printing) of thick graphene-based electrodes. Carbon N Y. 2017;119:257–266.

[137] Fieber L, Evans JD, Huang C, et al. Single-operation, multi-phase additive manufacture of electro-chemical double layer capacitor devices. Addit Manuf. 2019;28:344–353.

[138] Zhang C, Kremer MP, Seral-Ascaso A, et al. Stamping of flexible, coplanar micro-supercapacitors using MXene inks. Adv Funct Mater. 2018;28(9):1705506.

[139] Tang K, Ma H, Tian Y, et al. 3D printed hybrid-dimensional electrodes for flexible micro-supercapacitors with superior electrochemical behaviours. Virtual Phys Prototyp. 2020;15(sup1):511–519.

[140] Zhu C, Liu T, Qian F, et al. Supercapacitors based on three-dimensional hierarchical graphene aerogels with periodic macropores. Nano Lett. 2016;16(6):3448–3456.

[141] Zhao C, Wang C, Gorkin Iii R, et al. Three dimensional (3D) printed electrodes for interdigitated supercapacitors. Electrochem Commun. 2014;41:20–23.

[142] Xu Y, Zhang R, Harrison D, et al. Design and fabrication of modular supercapacitors using 3D printing; 2018.

[143] Nathan-Walleser T, Lazar IM, Fabritius M, et al. 3D micro-extrusion of graphene-based active electrodes: towards high-rate AC line filtering performance electrochemical capacitors. Adv Funct Mater. 2014;24(29):4706–4716.

[144] Sun G, An J, Chua CK, et al. Layer-by-layer printing of laminated graphene-based interdigitated microelectrodes for flexible planar micro-supercapacitors. Electrochem Commun. 2015;51:33–36.

[145] Li J, Mishukova V, Östling M. All-solid-state micro-supercapacitors based on inkjet printed graphene electrodes. Appl Phys Lett. 2016;109(12):123901.

[146] Chen B, Jiang Y, Tang X, et al. Fully packaged carbon nanotube supercapacitors by direct ink writing on flexible substrates. ACS Appl Mater Interfaces. 2017;9(34):28433–28440.

[147] Delekta SS, Smith AD, Li J, et al. Inkjet printed highly transparent and flexible graphene micro-supercapacitors. Nanoscale. 2017;9(21):6998–7005.

[148] Gao T, Zhou Z, Yu J, et al. 3D printing of tunable energy storage devices with both high areal and volumetric energy densities. Adv Energy Mater. 2019;9(8):1802578.

[149] Wang Z, Zhang QE, Long S, et al. Three-dimensional printing of polyaniline/reduced graphene oxide composite for high-performance planar supercapacitor. ACS Appl Mater Interfaces. 2018;10(12):10437–10444.

[150] Wang T, Li L, Tian X, et al. 3D-printed interdigitated graphene framework as superior support of metal oxide nanostructures for remarkable micro-pseudocapacitors. Electrochim Acta. 2019;319:245–252.

[151] Yu L, Fan Z, Shao Y, et al. Versatile N-doped MXene ink for printed electrochemical energy storage application. Adv Energy Mater. 2019;9(34):1901839.

[152] Yao B, Chandrasekaran S, Zhang J, et al. Efficient 3D printed pseudocapacitive electrodes with ultrahigh MnO2 loading. Joule. 2019;3(2):459–470.

[153] Idrees M, Ahmed S, Mohammed Z, et al. 3D printed supercapacitor using porous carbon derived from packaging waste. Addit Manuf. 2020;36:101525.

[154] Yao B, Chandrasekaran S, Zhang H, et al. 3D-printed structure boosts the kinetics and intrinsic capacitance of pseudocapacitive graphene aerogels. Adv Mater. 2020;32(8):1906652.

[155] Munuera JM, Paredes JI, Enterría M, et al. High performance Na-O2 batteries and printed microsupercapacitors based on water-processable, biomolecule-assisted anodic graphene. ACS Appl Mater Interfaces. 2019;12(1):494–506.

[156] Chae C, Kim Y-B, Lee SS, et al. All-3D-printed solid-state microsupercapacitors. Energy Storage Mater. 2021;40:1–9.

[157] Kaur I, Singh P. State-of-the-art in heat exchanger additive manufacturing. Int J Heat Mass Transfer. 2021;178:121600.

[158] Deisenroth DC, Moradi R, Shooshtari AH, et al. Review of heat exchangers enabled by polymer and polymer composite additive manufacturing. Heat Transfer Eng. 2018;39(19):1648–1664.

[159] Li Q, Li C, Du Z, et al. A review of performance investigation and enhancement of shell and tube thermal energy storage device containing molten salt based phase change materials for medium and high temperature applications. Appl Energy. 2019;255:113806.

[160] Ge R, Li Q, Li C, et al. Evaluation of different melting performance enhancement structures in a shell-and-tube latent heat thermal energy storage system. Renewable Energy. 2022;187:829–843.

[161] Liu Z, Yao Y, Wu H. Numerical modeling for solid–liquid phase change phenomena in porous media: shell-and-tube type latent heat thermal energy storage. Appl Energy. 2013;112:1222–1232.

[162] Righetti G, Savio G, Meneghello R, et al. Experimental study of phase change material (PCM) embedded in 3D periodic structures realized via additive manufacturing. Int J Therm Sci. 2020;153:106376.

[163] Almonti D, Mingione E, Tagliaferri V, et al. Design and analysis of compound structures integrated with bio-based phase change materials and lattices obtained through additive manufacturing. The Int J Adv Manuf Technol. 2022;119(1):149–161.

[164] Qureshi ZA, Al-Omari SAB, Elnajjar E, et al. On the effect of porosity and functional grading of 3D printable triply periodic minimal surface (TPMS) based architected lattices embedded with a phase change material. Int J Heat Mass Transfer. 2022;183:122111.

[165] Zhang T, Deng X, Zhao M, et al. Experimental study on the thermal storage performance of phase change materials embedded with additively manufactured triply periodic minimal surface architected lattices. Int J Heat Mass Transfer. 2022;199:123452.

[166] Ma J, Ma T, Cheng J, et al. 3D printable, recyclable and adjustable comb/bottlebrush phase change polysiloxane networks toward sustainable thermal energy storage. Energy Storage Mater. 2021;39:294–304.

[167] Li C, Li Q, Lu X, et al. Inorganic salt based shape-stabilized composite phase change materials for medium and high temperature thermal energy storage: ingredients selection, fabrication, microstructural characteristics and development, and applications. J Energy Storage. 2022;55:105252.

[168] Nofal M, Al-Hallaj S, Pan Y. Experimental investigation of phase change materials fabricated using selective laser sintering additive manufacturing. J Manuf Process. 2019;44:91–101.

[169] Nofal M, Al-Hallaj S, Pan Y. Thermal management of lithium-ion battery cells using 3D printed phase change composites. Appl Therm Eng. 2020;171:115126.

[170] Rigotti D, Dorigato A, Pegoretti A. 3D printable thermoplastic polyurethane blends with thermal energy storage/release capabilities. Mater Today Commun. 2018;15:228–235.

[171] Freeman TB, Messenger MA, Troxler CJ, et al. Fused filament fabrication of novel phase-change material functional composites. Addit Manuf. 2021;39:101839.

[172] Singh P, Odukomaiya A, Smith MK, et al. Processing of phase change materials by fused deposition modeling: toward efficient thermal energy storage designs. J Energy Storage. 2022;55:105581.

[173] Wei P, Cipriani CE, Pentzer EB. Thermal energy regulation with 3D printed polymer-phase change material composites. Matter. 2021;4(6):1975–1989.

[174] Feng C-P, Sun K-Y, Ji J-C, et al. 3D printable, form stable, flexible phase-change-based electronic packaging materials for thermal management. Addit Manuf. 2023;71:103586.

[175] Yang Z, Ma Y, Jia S, et al. 3D-printed flexible phase-change nonwoven fabrics toward multifunctional clothing. ACS Appl Mater Interfaces. 2022;14(5):7283–7291.

[176] Ma J, Ma T, Cheng J, et al. Polymer encapsulation strategy toward 3D printable, sustainable, and reliable form-stable phase change materials for advanced thermal energy storage. ACS Appl Mater Interfaces. 2022;14 (3):4251–4264.

[177] Markl M, Körner C. Multiscale modeling of powder bed–based additive manufacturing. Annu Rev Mater Res. 2016;46(1):93–123.

[178] Ge R, Flynn J. A computational method for detecting aspect ratio and problematic features in additive manufacturing. J Intell Manuf. 2022;33(2):519–535.

[179] Grant PS, Greenwood D, Pardikar K, et al. Roadmap on Li-ion battery manufacturing research. J Phys: Energy. 2022;4:042006.

[180] Gao X, Liu X, He R, et al. Designed high-performance lithium-ion battery electrodes using a novel hybrid model-data driven approach. Energy Storage Mater. 2021;36:435–458.

[181] Kim J-E, Park K. Multiscale topology optimization combining density-based optimization and lattice enhancement for additive manufacturing. Int J Precis Eng Manufacturing-Green Technol. 2021;8:1197–1208.

[182] Chen C-T, Chrzan DC, Gu GX. Nano-topology optimization for materials design with atom-by-atom control. Nat Commun. 2020;11(1):3745.

[183] Zheng X, Deotte J, Alonso MP, et al. Design and optimization of a light-emitting diode projection microstereolithography three-dimensional manufacturing system. Rev Sci Instrum. 2012;83(12):125001.

[184] Liu M, Wu F, Bai Y, et al. Boosting sodium storage performance of hard carbon anodes by pore architecture engineering. ACS Appl Mater Interfaces. 2021;13 (40):47671–47683.

[185] Chen J, Liu X, Tian Y, et al. 3D-Printed anisotropic polymer materials for functional applications. Adv Mater. 2022;34(5):2102877.